(4)

AFGL-TR-88-0146
ENVIRONMENTAL RESEARCH PAPERS, NO. 1006

Atmospheric Aerosol Scattering Background Observations

FRANK W. GIBSON

14 June 1988

OPTICAL PHYSICS DIVISION PROJECT 7670
AIR FORCE GEOPHYSICS LABORATORY
HANSCOM AFB, MA 01731

A

"This technical report has been reviewed and is approved for publication"

FOR THE COMMANDER

Donald E. Bedo

DONALD E. BEDO
Branch Chief

R. Earl Good

R. EARL GOOD
Division Director

This report has been reviewed by the ESD Public Affairs Office (PA) and is releasable to the National Technical Information Service (NTIS).

Qualified requestors may obtain additional copies from the Defense Technical Information Center. All others should apply to the National Technical Information Service.

If your address has changed, or if you wish to be removed from the mailing list, or if the addressee is no longer employed by your organization, please notify AFGL/DAA, Hanscom AFB, MA 01731. This will assist us in maintaining a current mailing list.

Do not return copies of this report unless contractual obligations or notices on a specific document requires that it be returned

UNCLASSIFIED
SECURITY CLASSIFICATION OF THIS PAGE

AD-A206 752

REPORT DOCUMENTATION PAGE

Form Approved OMB No. 0704-0188

1a. REPORT SECURITY CLASSIFICATION Unclassified	1b. RESTRICTIVE MARKINGS
2a. SECURITY CLASSIFICATION AUTHORITY	3. DISTRIBUTION / AVAILABILITY OF REPORT Approved for public release; distribution unlimited.
2b. DECLASSIFICATION / DOWNGRADING SCHEDULE	
4. PERFORMING ORGANIZATION REPORT NUMBER(S) AFGL-TR-88-0146 ERP, No. 1006	5. MONITORING ORGANIZATION REPORT NUMBER(S)
6a. NAME OF PERFORMING ORGANIZATION Air Force Geophysics Laboratory 6b. OFFICE SYMBOL (If applicable) OPA	7a. NAME OF MONITORING ORGANIZATION
6c. ADDRESS (City, State, and ZIP Code) Hanscom AFB Massachusetts 01731-5000	7b. ADDRESS (City, State, and ZIP Code)
8a. NAME OF FUNDING / SPONSORING ORGANIZATION 8b. OFFICE SYMBOL (If applicable)	9. PROCUREMENT INSTRUMENT IDENTIFICATION NUMBER
8c. ADDRESS (City, State, and ZIP Code)	10. SOURCE OF FUNDING NUMBERS PROGRAM ELEMENT NO. 62101F; PROJECT NO. 7670; TASK NO. 15; WORK UNIT ACCESSION NO. 16

11. TITLE (Include Security Classification)
Atmospheric Aerosol Scattering Background Observations

12. PERSONAL AUTHOR(S)
Frank W. Gibson

13a. TYPE OF REPORT	13b. TIME COVERED	14. DATE OF REPORT (Year, Month, Day)	15. PAGE COUNT
Scientific Interim	FROM _____ TO _____	1988 June 14	38

16. SUPPLEMENTARY NOTATION

17. COSATI CODES			18. SUBJECT TERMS (Continue on reverse if necessary and identify by block number)
FIELD	GROUP	SUB-GROUP	Aerosol particles, turbidity, phase function, Angular scattering, polarization . (MSP)

19. ABSTRACT (Continue on reverse if necessary and identify by block number)

Optical scattering, under very clear atmospheric conditions, was measured in situ and analyzed. The experiments were made with a large balloonborne nephelometer launched from Holloman AFB, New Mexico and flown to 26 km altitude. Profiles of angular scattering and polarization properties of atmospheric aerosols show contrast with aerosol particles encountered in the troposphere and stratosphere. The results are compared with those obtained using particle counters under similar atmospheric conditions.

(1)

20. DISTRIBUTION/AVAILABILITY OF ABSTRACT	21. ABSTRACT SECURITY CLASSIFICATION
☐ UNCLASSIFIED/UNLIMITED ☒ SAME AS RPT. ☐ DTIC USERS	Unclassified
22a. NAME OF RESPONSIBLE INDIVIDUAL Frank W. Gibson	22b. TELEPHONE (Include Area Code) (617) 377-3092
	22c. OFFICE SYMBOL OPA

DD FORM 1473, JUN 86 *Previous editions are obsolete.*

SECURITY CLASSIFICATION OF THIS PAGE
UNCLASSIFIED

Contents

Illustrations

Tables

Atmospheric Aerosol Scattering Background Observations

1. INTRODUCTION

Of particular importance to the problem of electro-optical (E/O) propagation in the terrestrial atmosphere is the question of the existence of atmospheric aerosols at all altitudes that may affect such propagation. A series of balloon flights with a large polar nephelometer provides results that consistently indicate the presence of aerosol particles, even during periods relatively free of volcanic dust incursions. Measurable scattering properties of aerosols were observed in both the troposphere and stratosphere and no region was found to be aerosol-free.

The thrust of this report is therefore to demonstrate that ground-based E/O systems operating in the visible spectral range such as LIDARS will give unreliable results if it is assumed that regions identified by minima in backscatter contain no aerosols. Similarly, very small particles (Aitken nuclei) cannot be excluded as sources of error for systems operating at wavelengths below about 0.5 μm, because they are virtually undetectable by LIDAR alone, although they are ubiquitous and may exist in large number concentrations, even in very clear air. Scattering from small particles is not a trivial problem, when molecular scattering is considered as a calibration threshold in remote aerosol or molecular density measurements. Any contribution from these particles results in some error, if the instrumentation cannot distinguish between small particles and air molecules.

Finally, two sets of in-situ data from the balloon-borne nephelometer show contrasting scattering behavior for high concentrations of small particles in one case and very low concentrations of large particles (> 0.15 μm) in the other, for regions in the troposphere assumed to be

---

(Received for Publication 14 June 1988).

virtually aerosol-free by some investigators.[1,2,3,4] Inferences from these results are compared with those obtained using particle-counting methods.

2. OBSERVATIONS

The balloon-borne nephelometer has been described in previous publications.[5,6,7] The primary components of the instrument were a 150-W xenon light source and five photometers all mounted on an optically rigid frame so as to measure the scattered light at 15, 30, 50, 100, and 150°, from a defined volume (about 250 cm^3) of atmosphere. Spectral filters at 0.475, 0.515, 0.660, and 0.745 μm in the photometers were used to examine the properties of the scattered light in the visible region. In addition, the polarization at 0.475 and 0.660 μm was analyzed for the 50, 100, and 150° scattering angles. A series of balloon flights using the equipment measured the altitudinal variability in scattering properties of atmospheric aerosols.

The optical parameters least affected by instrument calibration on the one hand and most sensitive to atmospheric aerosol scattering characteristics on the other, are the polarization of the scattered light and the dissymmetry in angular scattering as a function of altitude. At scattering angles near 90°, the polarization is maximized by scattering from air molecules so that a reduction in polarization is attributed to atmospheric aerosols. Similarly, the ratio of forward-to-backward scattering or the so-called dissymmetry parameter, senses the enhanced forward scattering due to aerosols as opposed to the characteristic angular symmetry of molecular scattering. Together with the absolute scattering intensity data, these two parameters provide a means for identifying the vertical structure of atmospheric aerosols using optical diagnostic techniques.

Some experimental results from previous balloon flights have been published as noted above. The objective here is to highlight certain aspects of these data, and to include previously unpublished data, in an attempt to provide evidence for the existence of a background of aerosols in the atmosphere. These results are pertinent because they were obtained during periods that were relatively free from volcanic dust contamination of the stratosphere and might be considered

---

1. Northam, G.B. et. al. (1974) Dustsonde and lidar measurements of stratospheric aerosols: a comparison, *Appl. Opt.* **13**:2416-2421.
2. Russell, P.B. et. al. (1975) Results of stratospheric lidar observations, *Fourth Conference on the Climatic Impact Assessment Program*, Cambridge, MA, 4-7 February.
3. McCormick, M.P. and Fuller, W.H. (1975) Lidar measurements of intense stratospheric dust layers, *Appl. Opt.* **14**:4-5.
4. Barteneva, O.D. (1960) Scattering functions of light in the atmospheric boundary layer, *Bull. Acad. Sci. USSR Geophys. Sci.*, 1237-1244.
5. Gibson, F.W. and Dearborn, F.K. (1971) *Atmospheric Optics Measurements with a Balloon-Borne Nephelometer*, AFCRL-TR-71-0455, AD736408.
6. Gibson, F.W. and Volz, F.E. (1972) High altitude measurements of the optical-scattering properties of the atmosphere, presented at Optical Society of America Meeting, New York, NY, April.
7. Gibson, F.W. (1976) In-situ photometric observations of angular scattering from atmospheric aerosols, *Appl. Opt.* **15**:2520-2533.

representative of "normal" conditions for altitudes up to 26 km. The last balloon flight was made from Holloman AFB, New Mexico in June 1976, approximately two years after the incursion of volcanic dust from the eruption of Fuego in Guatemala in October 1974.[8]

2.1 Turbidity

Figure 1 is a plot of turbidity as a function of altitude and wavelength. This profile was obtained by using the 50° scattering intensity data to separate the molecular from aerosol scattering. A typical plot of the intensity, presented as the volume scattering function, is shown in Figure 2. The latter profile, $\beta_T(50°)$ is due to both aerosol and molecular scattering. Single scattering is assumed so that the intensities are separable and additive. The total intensity is

$$\beta_T = \beta_R + \beta_A \tag{1}$$

where β_R = volume scattering function due to molecular or Rayleigh particles

$[cm^{-1}\ sr^{-1}]$.

$\beta_A \equiv$ volume scattering function due to aerosol particles $[cm^{-1}\ sr^{-1}]$

Generally,

$$\beta_T(\phi_s) = \sigma_R P_R(\phi_s) + \sigma_A P_A(\phi_s) \tag{2}$$

where σ_R and σ_A are respectively the Rayleigh and aerosol scattering coefficients $[cm^{-1}]$ and P_R, P_A are the Rayleigh and aerosol phase functions $[sr^{-1}]$. The rationale for this formulation follows from the empirical and theoretical observations that the Rayleigh and aerosol phase functions, at approximately 50° scattering angle, are linearly related for aerosol size distributions found in clear air. Barteneva[4] has shown that the phase function for aerosols, associated with atmospheric conditions of high visibility, intersect in the vicinity of 50°. Thus

$$\frac{\beta_T}{\beta_R} - 1 = \frac{\beta_A(50°)}{\beta_R(50°)} = \frac{\sigma_A P_A(50°)}{\sigma_R P_A(50°)} = C\frac{\sigma_A}{\sigma_R}\ . \tag{3}$$

Since $C \simeq 1$, we obtain the turbidity τ, a quantity proportional to the relative number of aerosols to molecules, given by

$$t \simeq \frac{\beta_T}{\beta_R} - 1 = \frac{\sigma_A}{\sigma_R}\ . \tag{4}$$

In Figure 1 particular notice might be given to the low values of turbidity encountered near the tropopause at approximately 10 km since this minimum is characteristic of LIDAR observations. However further comments will be made after a more detailed analysis is presented later.

---

8. Meinel, A.B. and Meinel, M.P. (1975) A stratospheric dust event of November 1974, *Science* **188**:477-481.

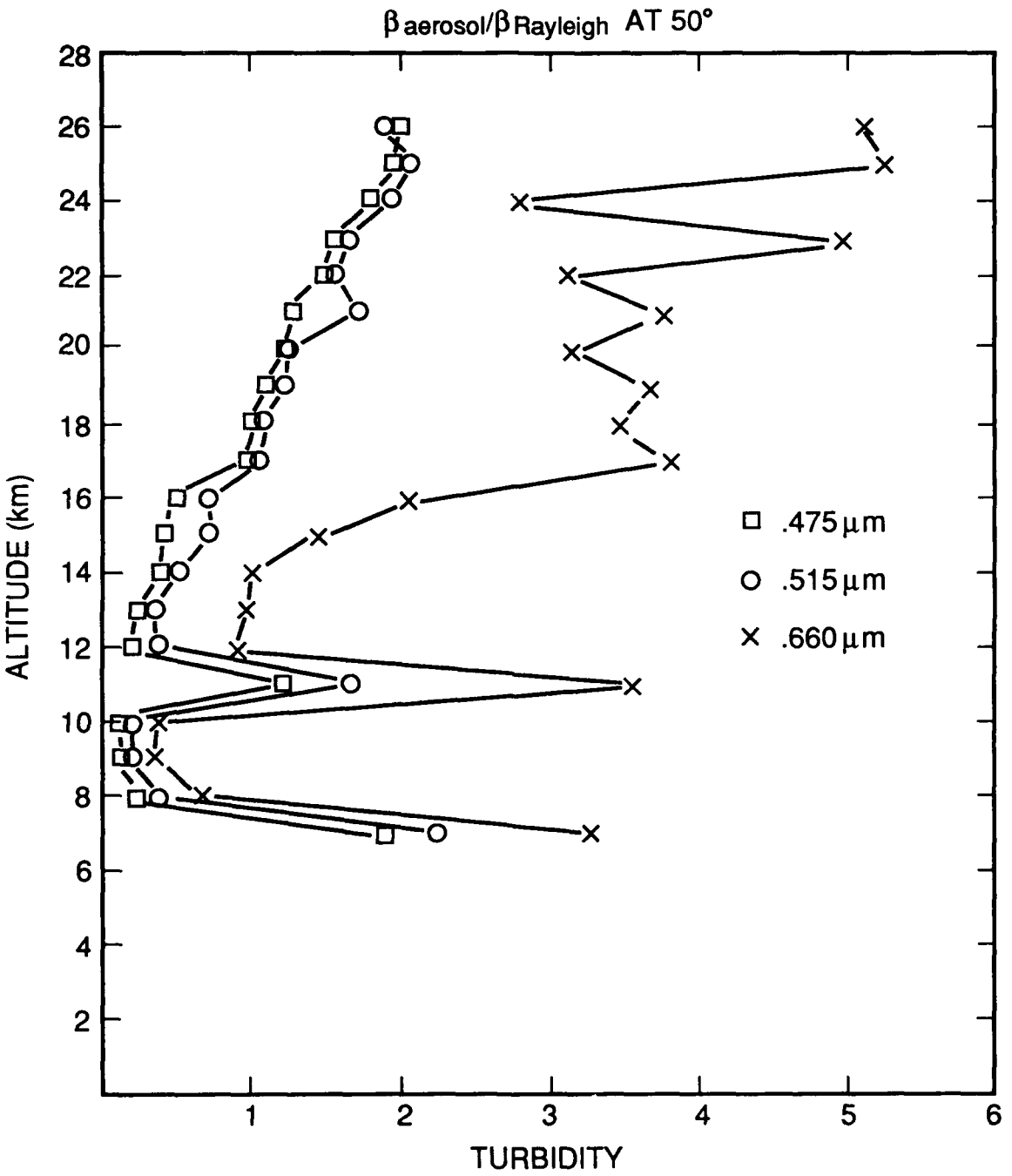

Figure 1. Turbidity σ_A/σ_R vs Altitude (June 1976)

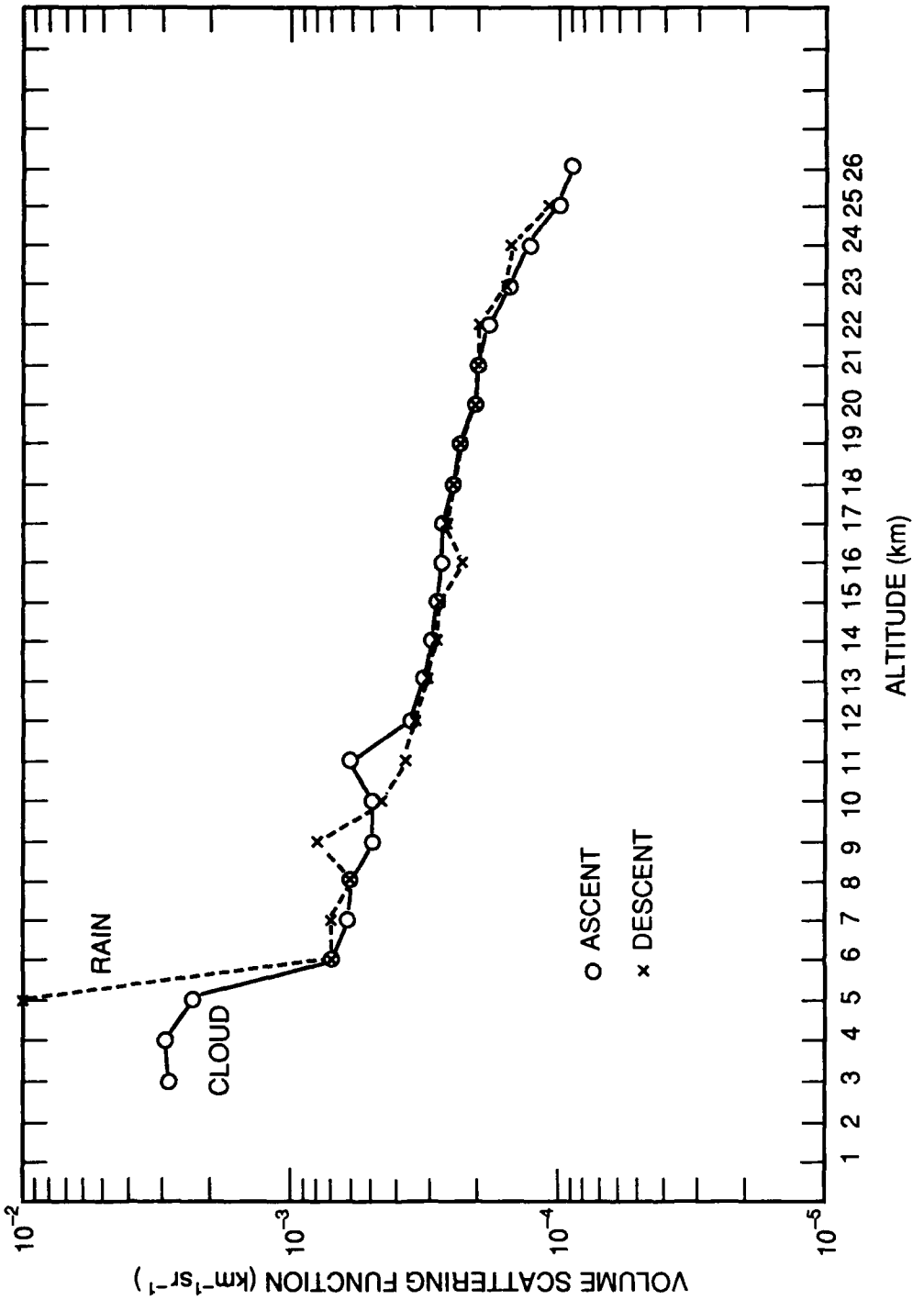

Figure 2. 50° Volume Scattering Functions vs Altitude at 515 μm Wavelength

An earlier flight in November, 1970[5] resulted in the turbidity profile shown in Figure 3. Although the values found in the stratosphere (designated the Junge aerosol layer[9]) were very close to those observed in 1976, the tropospheric values were strikingly different. An explanation for the differences is given later in this report and only the close comparison of the stratospheric data, particularly at 0.660 μm wavelength, is emphasized at this juncture. The latter comparison is particularly meaningful because of the duration of about six years between flights; a period that included a major volcanic eruption; that is, the Fuego event.[8]

2.2 Polarization

Figure 4 is a plot of the polarization ratio for the 1976 flight. This profile was determined by taking the ratio of 100° scattered light at 0.475 μm, measured sequentially through the filters containing linear polarizers. The polarizers were oriented so as to detect the vertical and horizontal components of the scattered light. Figure 5 is a similar plot for the 1970 data, but the photometer was located at the 90° scattering angle. In these profiles, the parameter displayed is related to the degree of linear polarization by

$$\text{Pol.} = \frac{I_V - I_H}{I_V + I_H} = \frac{I_V/I_H - 1}{I_V/I_H + 1} \tag{5}$$

where I_V and I_H are the scattered intensities perpendicular and parallel to the plane of scattering and the quantity I_V/I_H is an absolute measurement, because, for a specific photometer/detector, the calibration factor is common to I_V and I_H. Further analysis of this parameter has been given in previous publications[7] and the profiles are presented here primarily to illustrate differences in the observations for the two flights as well as to indicate the consistency between the polarization ratio and other data, such as turbidity profiles. In terms of comparison, the 1976 data indicate the presence of large, so called, Mie[9] particles, at virtually all altitudes inasmuch as the polarization ratio reaches peak values between 7 and 8 in the 9 - 10 km region, which coincides with the turbidity minimum. This maximum corresponds to 76 percent polarization of the scattered light. An aerosol-free region requires a ratio of about 14 (87 percent polarization) which would indicate pure molecular scattering. The 1970 data in Figure 5 show maxima between 9 and 10 at several points in the 5 - 10 km altitude range, indicating about 82 percent polarization, while molecular scattering would give an I_V/I_H value of 24, that is, 92 percent polarization for the 90° scattering angle. In both profiles however, the ratios are approximately the same for the Junge layer, above 16 km, when the 10° difference in photometer location is considered. That is, a comparable reduction in polarization occurred when the stratospheric Mie particles were encountered. Noteworthy also is that such reduction (to virtually the same value) also occurred in the troposphere for the 1976 data, thereby suggesting large particles were present, which affected the polarization in much the same manner as those in the stratosphere.

---

9. Junge, C.E., Chagnon, C.W., and Manson, J.E. (1961) Stratospheric aerosols, *J. Meteorol.* **18**: 81-98.

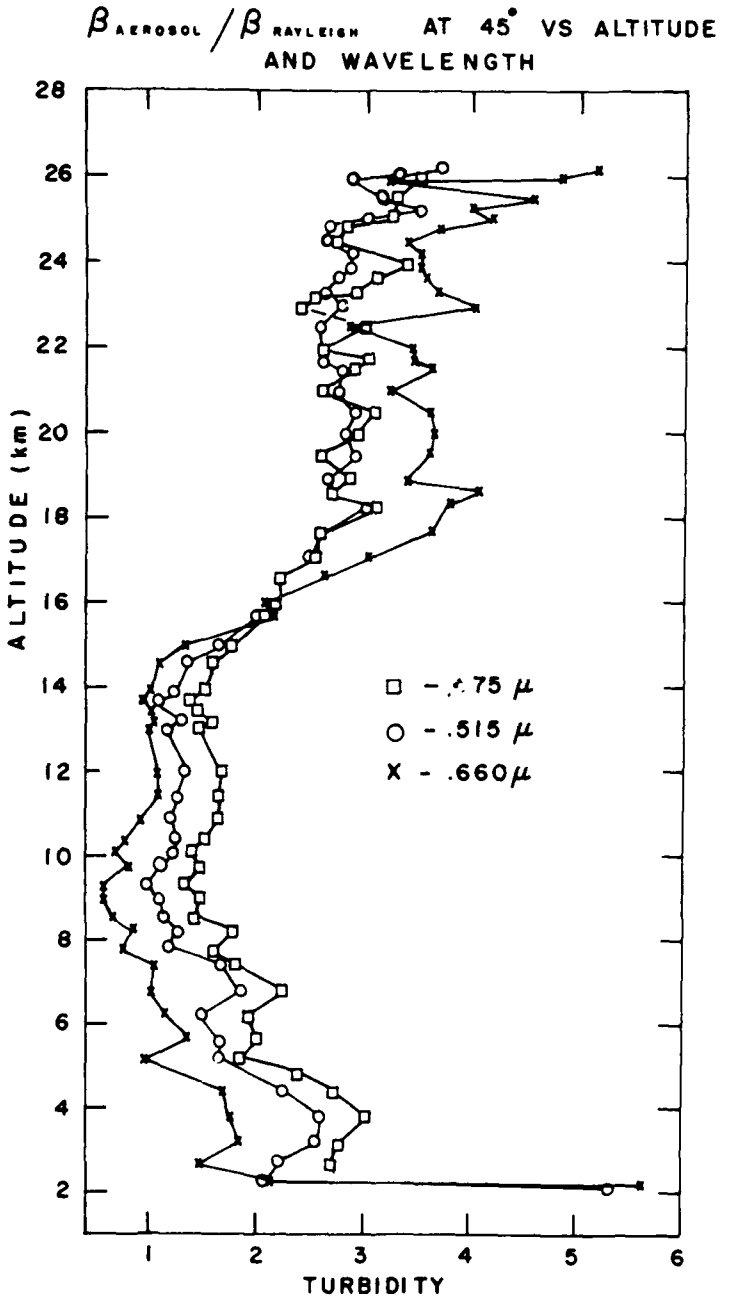

Figure 3. Turbidity σ_A/σ_R vs Altitude (November 1970)

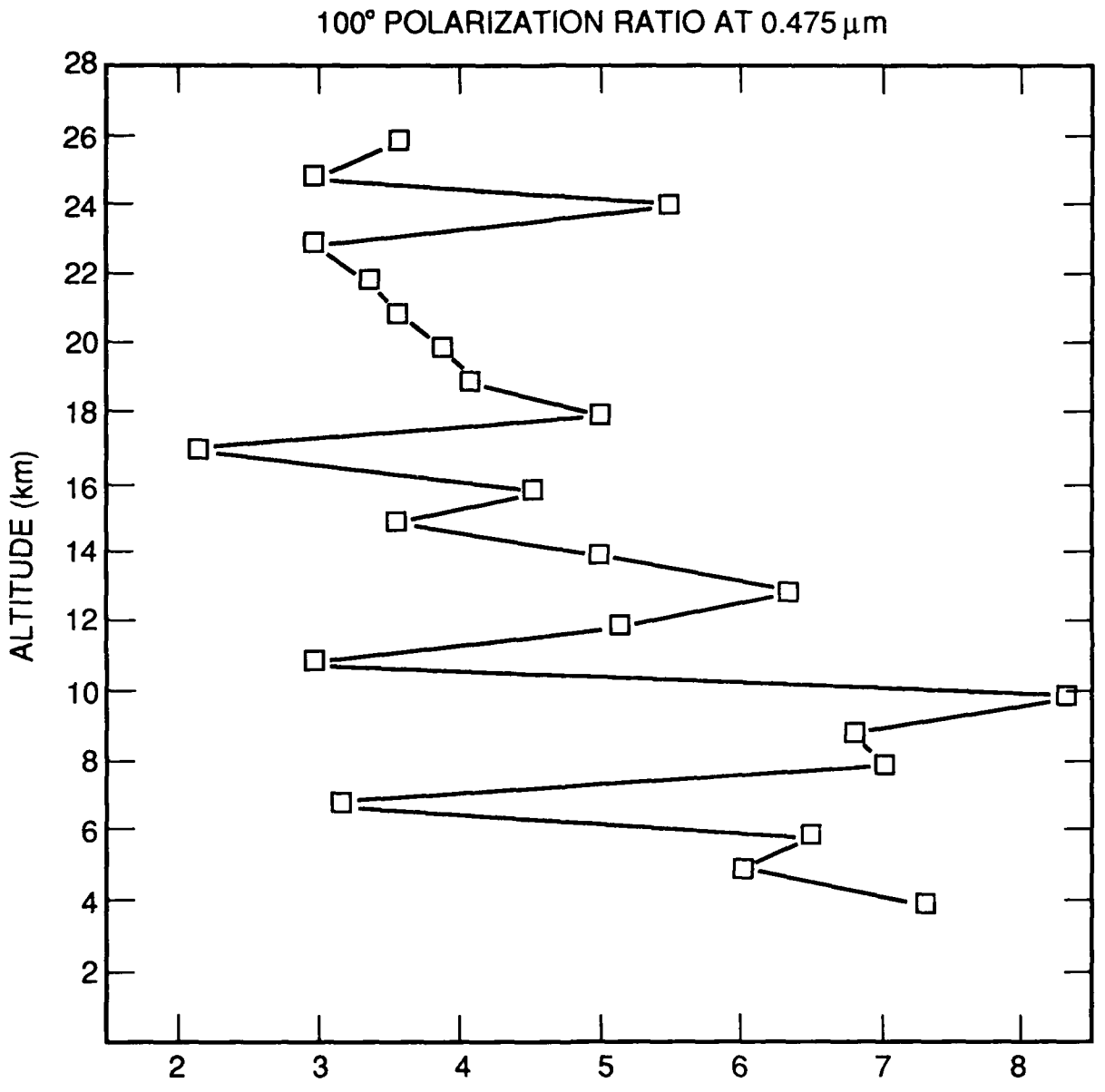

Figure 4. 100° Polarization Ratio vs Altitude (June 1976)

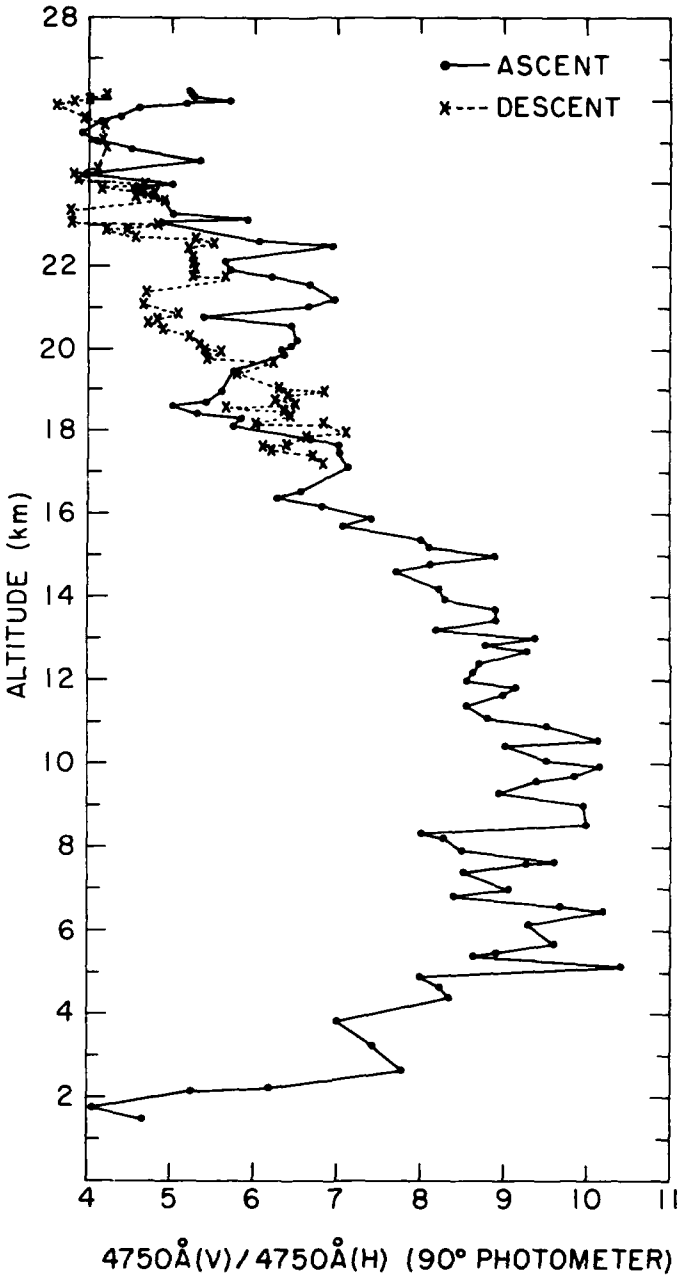

Figure 5. 90° Polarization Ratio vs Altitude (November 1970)

2.3 Dissymmetry

It has been shown[7] that the ratio of scattering intensities for two symmetric scattering angles can be related to the turbidity as a function of altitude and as a result a parameter is obtained that indicates the altitudinal variability in angular scattering by aerosol particles. The symmetric angles utilized in the nephelometer flights were 30° and 150° and thus the dissymmetry is defined as:

$$R \equiv \frac{\beta_\lambda(30°)}{\beta_\lambda(150°)} = \frac{P_R\lambda\,(30°) + (\sigma_A/\sigma_R)\,P_A\lambda\,(30°)}{P_R\lambda\,(150°) + (\sigma_A/\sigma_R)\,P_A\lambda\,(150°)} \tag{6}$$

where

$R \equiv$ dissymmetry factor or simply the forward-to-backscatter ratio,

$P_R\lambda \equiv$ normalized Rayleigh phase function,

$P_A\lambda \equiv$ normalized aerosol phase function, and

$\sigma_A/\sigma_R = \tau$, the turbidity (a quantity independent of scattering angle).

Now $P_R\lambda\,(30°) = P_R\lambda\,(150°)$ because Rayleigh scattering is symmetric relative to the 90° scattering angle. Aerosol particles with a size parameter, $X = \frac{2\pi r}{\lambda} > 0.8$, scatter more light in the forward direction[10] which means $P_A\lambda\,(30°) > P_A\lambda\,(150°)$. Consequently, $R > 1$ when $\tau > 0$, with the result that the presence of aerosols should be evidenced by values of the R-parameter greater than unity. Moreover, this factor is wavelength dependent, because the turbidity varies with wavelength, and it will be shown in the next section that such wavelength dispersion provides quantitative information on the aerosol phase function.

The vertical profile of R for the 1976 flight is shown in Figure 6. This plot is simply the ratio of the experimentally determined scattering functions, $\beta\lambda\,(30°)/\beta\lambda\,(150°)$, at the 30 and 150° angles, and the 0.475, 0.515, and 0.660 μm values are displayed. This profile is clearly very similar in overall structure to the turbidity plot shown in Figure 1 suggesting a correlation between R and τ as predicted by Eq. (6). The Junge layer is delineated in particular by the R-parameter with peak values occurring at about 18 km, and prominent dispersion toward the red, (0.660 μm).

3. DISCUSSION OF THE OBSERVATIONS

3.1 Theoretical Considerations

More quantitative interpretations of the data from the balloon-borne nephelometer experiments require an outline of applicable theory. These concepts are either extensions of or direct use of Rayleigh and Mie scattering theory, which have served to explain atmospheric light scattering phenomena generally.

---

10. Van de Hulst, H.C. (1957) *Light Scattering by Small Particles*, John Wiley & Sons, New York.

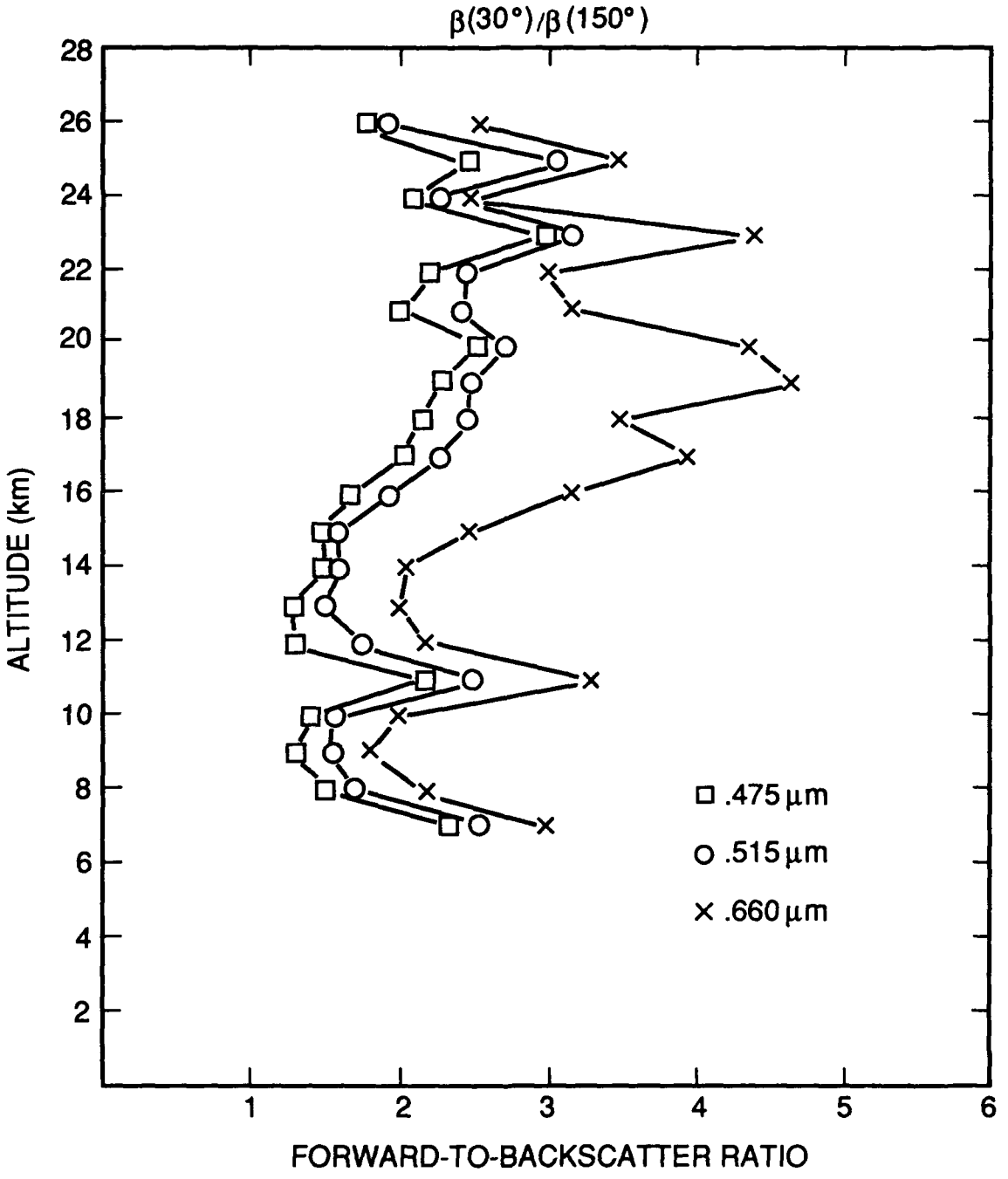

Figure 6. The Ratio of Forward-to-Backward Scattering (Dissymmetry) vs Altitude (June 1976)

In view of the fact that very small atmospheric particles cover a size range from air molecules ($\simeq 3 \times 10^{-4}$ μm) to condensation nuclei or Aitken particles ($\simeq 10^{-2}$ μm) it is necessary to examine Rayleigh scattering as a function of particle size. Van de Hulst[10] has shown that when the particle size parameter,

$$X = \frac{2\pi r}{\lambda} < 0.8,$$

the angular scattering pattern is virtually symmetrical. Recent laboratory studies with laser light have also verified that negligible error will be introduced when this upper limit is assumed for the size parameter of Rayleigh scatterers.[11] The implication for the balloon-borne nephelometer is that at $\lambda = 0.475$ μm, atmospheric particles with radii less than 0.06 μm can be considered to be Rayleigh scatterers. This limit therefore includes Aitken nuclei, which are apparently critical to cloud formation and have been observed in the troposphere with number concentrations the order of 10^4 cm^{-3}. The Rayleigh scattering formula is usually[12] expressed as

$$f_R(\phi, \lambda) = \frac{9}{2}\pi^2 n_R \left(\frac{m^2 - 1}{m^2 + 2}\right)^2 \frac{v^2}{\lambda^4} (1 + \cos^2 \phi) \, [cm^{-1} - sr^{-1}] \tag{7}$$

where

f_R = angular volume scattering function

n_R = number particles cm^3

m = refractive index

v = volume of particles

λ = wavelength of scattered light

ϕ = scattering angle

For spherical particles (such as, air molecules) this equation becomes

$$f_R(\phi, \lambda) = 8\pi^4 \left(\frac{m^2 - 1}{m^2 + 2}\right)^2 \frac{n_R r^6}{\lambda^4} (1 + \cos^2 \phi) \, [cm^{-1} - sr^{-1}] \tag{8}$$

where r = radius of particles, assumed to be monodispersed. The scattering function is therefore proportional to the 6th power of particle radius. Indeed, Lord Rayleigh originally determined the λ^{-4} wavelength dependence from dimensional considerations. That is, the scattering intensity is proportional to the square of the particle volume and the number density, and the λ-dependence of λ^{-4} is required for the intensity to have the proper dimensions.

---

11. Sassen, K. (1981) Infrared (10.6 μm) scattering and extinction in laboratory water and ice clouds, *Appl. Opt.* **20**:185-193.
12. Kerker, M. (1969) *The Scattering of Light and Other Electromagnetic Radiation*, Academic Press, New York.

Because one of the objectives in this report is to emphasize the importance of the r^6 factor in Rayleigh scattering formulations, it is informative to illustrate that this relationship can also be deduced from Mie scattering considerations. Bullrich[13] has examined the scattering properties of atmospheric aerosols that have number densities which follow a power-law type distribution in size. Such distributions were found by Junge[9] in balloon-borne investigation[5] of naturally occurring aerosols and are given by

$$\frac{dn}{d(\log r)} = C r^{-\nu} \ [cm^{-3}] \quad . \tag{9}$$

This distribution gives the number of particles dn with radius between r and (r + dr). This can be rewritten in the form

$$\frac{dn}{dr} = 0.434\, C r^{-(\nu+1)} \ [cm^{-4}] \quad . \tag{10}$$

where the change of variable is, $d(\log r) = \frac{dr}{r}\frac{1}{\ln(10)} = 0.434\,\frac{dr}{r}$.

For such a size distribution Bullrich determines the scattering function to be

$$f_A(\phi, \lambda) = 0.434\,\frac{C}{2}\left(\frac{2\pi}{\lambda}\right)^{\nu-2} \int_{x_1}^{x_2} \frac{i(\phi, \lambda)}{x^{\nu+1}}\, dx \ [cm^{-1} - sr^{-1}] \tag{11}$$

where $x = \frac{2\pi r}{\lambda}$, is the size parameter. The integral

$$\int_{x_1}^{x_2} \frac{i(\phi, \lambda)}{x^{\nu+1}}\, dx = \eta(\phi, \lambda) \tag{12}$$

is the angle dependent factor or phase function that gives the angular scattering behavior in terms of the size parameter, which is dimensionless. This factor $\eta(\phi, \lambda)$ can be calculated for a given size distribution and wavelength, using Mie scattering computer codes. The constant, C, is determined from the total number of particles in a particular size range. That is, the total number N, of particles between r_1 and r_2 is

$$N = \int_{r_1}^{r_2} dn = 0.434\, C \int_{r_1}^{r_2} r^{-(\nu+1)}\, dr, \text{ from Eq. (10).}$$

Integration gives

$$N = \frac{0.434\, C}{\nu\, r_1^{\nu}}\left[1 - \left(\frac{r_1}{r_2}\right)^{\nu}\right] \tag{13}$$

---

13. Bullrich, K. (1964) Scattered radiation in the atmosphere and the natural aerosol, *Advances in Geophysics* **10**:101-257.

If $r_1 << r_2$, then $N \simeq 0.434\, C\, \frac{1}{\nu\, r_1^{\nu}}$ and for some r_1 and r_A,

$$C \simeq \frac{N\nu r_A^{\nu}}{0.434} \quad . \tag{14}$$

When this value is used in Eq. (11) we obtain

$$f_A(\phi, \lambda) \simeq \frac{N}{2} \left(\frac{2\pi}{\lambda}\right)^{\nu-2} \nu r_A^{\nu} \eta(\phi, \lambda) \quad . \tag{15}$$

For $\nu = 6$ we get

$$f_A(\phi, \lambda) \simeq 3N \left(\frac{2\pi}{\lambda}\right)^4 r_A^6\, \eta(\theta, \lambda) = 3N \frac{16\pi^4}{\lambda^4}\, r_A^6\, \eta(\phi, \lambda) \quad .$$

The explicit dependence of f_A, on λ^{-4} and r_A^6 is clear. Although Eq. (15) will be applied later in the analysis of the turbidity data, the special case $\nu = 6$ simply illustrates the consistency between Rayleigh and Mie theory in the domain of small particles. It should be noted however that the radius exponent and the wavelength exponent are both functions of ν. That is, from Eq. (15),

$$f_A \sim \lambda^{-\nu+2} = \lambda^{-\alpha},$$

where $\alpha = \nu - 2$
and ν is the exponent in the power-law size distribution. This wavelength factor is the well-known Angstrom relation and has undergone extensive empirical verification, particularly under conditions where an exponential size distribution was apparent.

3.2 A Postulated Size Distribution

Because optical scattering effects of very small aerosols are usually neglected, since they have little effect on visibility, few experimental data exist relevant to their influence on atmospheric scattering when large particles are virtually absent, that is, under very clear sky conditions. To assess such an environment we constructed a particle size distribution with a dearth of particles greater than 0.1 μm in radius.

An inverse power-law distribution of the type suggested in Eq. (9) with the exponent $\nu = 6$, implies a constant slope or drop-off in particle radius from about 0.04 μm to approximately 0.07 μm. However, actual measurements of Aitken particles by Junge[14] and others[15,16], have indicated that such particles exhibit a log normal size distribution, probably due to coagulation of particles with radius less than about 0.02 μm. Moreover, particles with radii greater than this lower limit comprise the

---

14 Junge, C.E. (1961) Vertical profiles of condensation nuclei in the stratosphere, *J. Meteorol.* **18**:501-509.

15. Went, F.W. (1964) The nature of Aitkin condensation nuclei in the atmosphere, *Nature* **51**:1259-1267.

16. Whitby, K.T. (1975) *Modeling of Atmospheric Aerosol Particle Size Distribution*, Prog. Rep. 253, Particle Technology Laboratory, Univ. of Minnesota, Minneapolis.

bulk of the active condensation nuclei in the formation of clouds.[17] Investigations[17] into the process of water vapor condensation involve the so-called Kelvin factor, which indicates that condensation (that is, clouds, fog, etc) cannot begin on particles less than about 0.02 μm radius due to an abnormally high degree of supersaturation required. Under normal meteorological conditions in the atmosphere, hygroscopic nuclei serve as the centers on which water vapor condenses. Indeed, several studies have established correlations between spectra of cloud particles and those of small aerosol particles from which they evolve, depending upon factors such as relative humidity and supersaturation. In this connection Nilsson[18] has used a log normal size distribution given by

$$\frac{dn}{d(\log r)} = \frac{2.3N_T}{\sqrt{2\pi}\ \ln SG}\left[\exp - \frac{1}{2}\left(\frac{\ln r/rm}{\ln SG}\right)^2\right] \tag{16}$$

where $\frac{dn}{d(\log r)}$ = number density per log radius interval [cm^{-3}]

N_T = total number density [cm^{-3}]

r_m = median particle radius [μm]

$\ln SG$ = standard deviation of ln r.

To determine an appropriate distribution for the size range of small particles being considered it is only necessary to define ln SG so that most of the particles will have radii in the range 0.02 μm < r < 0.07 μm. This can be accomplished by matching the power-law distribution which dropped off as r^{-6}, and the log normal distribution at an initial value n_{ro} and at r = 0.07 μm. That is, the respective distributions have the form

$$\frac{dn}{d(\log r)} = n_{ro}\left(\frac{ro}{r}\right)^6 \tag{17}$$

and $$\frac{dn}{d(\log r)} = n_{ro}\left[\exp - \frac{1}{2}\left(\frac{\ln r/rm}{\ln SG}\right)^2\right], \text{ where } n_{ro} = \frac{2.3N_T}{\sqrt{2\pi}\ln SG} \tag{18}$$

If we then set

$$\left(\frac{ro}{r}\right)^6 = \left(\frac{r}{ro}\right)^{-6} = \exp - \frac{1}{2}\left(\frac{\ln r/ro}{\ln SG}\right)^2 \tag{19}$$

we obtain

$$6 \ln (r/ro) = -\frac{1}{2}\left(\frac{\ln r/ro}{\ln SG}\right)^2 \tag{20}$$

and

$$\ln SG = 0.289\sqrt{\ln (r/ro)}\ . \tag{21}$$

---

17. Junge, C.F. and McLaren, E. (1971) Relationship of cloud nuclei spectra to aerosol size distribution and composition, *J. Atmos. Sci.* **28**:382-390.

18. Nilsson, B. (1979) Meteorological influence on aerosol extinction in the 0.2 μm - 40 μm wavelength range, *Appl. Opt.* **18**:3457-3473.

Now assuming $r \leq 0.07$ μm and considering $r_o = 0.04$ μm as the median radius we find

$$\ln SG = 0.216$$

as the standard deviation, or the spread of our distribution, with a 2(ln SG) value (containing 95 percent of the particles) of

$$0.026\ \mu m < r < 0.062\ \mu m .$$

A representative value or n_{ro} from the measurements of Junge is

$$n_{ro} \simeq 5 \times 10^4/cm^3 \text{ at } r_o = 0.04\ \mu m .$$

The tropospheric model suggested by Shettle and Fenn[19] [converted to dn/d(log r)] has $n_{ro} = 1.07 \times 10^4/cm^3$ at r = 0.04 μm for a log normal distribution with $\sigma = 0.35$ and $N_T = 10^4/cm^3$. The distribution suggested here gives $N_T = 1.17 \times 10^4/cm^3$, for $n_{ro} = 5 \times 10^4/cm^3$. The total number of particles is thus close to those in other models, but the size distribution is restricted to particles less than 0.1 μm in radius. Such a restriction does not seem unreasonable for extremely clear air, such as that found in the desert environment of New Mexico.

The suggested size distribution was used to determine the pertinent scattering parameters using AFGL Mie codes. The angular symmetry and high degree of polarization at 90° demonstrated a scattering pattern with distinctive Rayleigh characteristics. The computed values of volume scattering functions were:

$1.94 \times 10^{-4}\ km^{-1}\ sr^{-1}$ at 0.475 μm

$1.42 \times 10^{-4}\ km^{-1}\ sr^{-1}$ at 0.515 μm

$5.30 \times 10^{-5}\ km^{-1}\ sr^{-1}$ at 0.660 μm .

These results clearly indicate a λ^{-4} dependence upon wavelength within less than 2 percent error. Finally, this distribution of small particles would give an expected value of turbidity of 0.34 at the 10 km altitude level often cited as a region of minimum scattering. However, these particles alone could not account for the abnormal dispersion in turbidity observed in 1970 because of the λ^{-4} dependence. Nonetheless, the resulting contribution to the total scattering cannot be assumed to be insignificant since it would introduce an error of at least 30 percent if this region were considered aerosol free. For the nephelometer data, such high cencentrations of small particles provide an additive factor that is examined qualititively in the next section to show that under these conditions the normal Angstrom relation is modified.

3.3 Small Particle Effects on the Observations

The postulated distribution has virtually no particles with radii greater than 0.1 μm. A more realistic picture of atmospheric aerosol particles would include some particles > 0.1 μm in radius,

---

19. Shettle, E.P. and Fenn, R. W. (1979) *Models for the Aerosol of the Lower Atmosphere and the Effects of Humidity Variations on their Optical Properties*, AFGL-TR-79-0214, ADA085951.

particularly in view of the well-documented enhanced concentration of large particles above the tropopause, that comprises the Junge layer in the stratosphere. It is therefore reasonable to expect a small number of these aerosols to be found below the tropopause due to atmospheric dynamics as well as settling processes. Because the sources of small particles and large particles are assumed uncorrelated and independent, the size distribution suggested here is bimodal. Other investigators[20,21] were compelled by their experimental data on sky radiation and absorption to postulate the existence of steep size distributions of small particles along with independent distributions of large particles. That a comparable situation existed in the troposphere during the 1970 balloon-borne nephelometer flight was suggested as an explanation for the "unusual" dispersion that resulted when the turbidity was plotted as a function of wavelength as seen in Figure 3.

The basic approach in analyzing the 1970 turbidity data was to assume that the turbidity emanated from non-molecular Rayleigh particles and Mie particles, that is, those with radii > 0.1 μm. Because the scattering intensities are separable, the observed volume scattering function for a bimodal distribution of aerosol is,

$$\beta_{Aobs} = \beta_P + \beta_A \tag{22}$$

where

β_P = volume scattering function for Rayleigh particles

β_A = volume scattering function for Mie particles

the observed turbidity is then,

$$\left(\frac{\beta_A}{\beta_R}\right)\text{Obs} = \left(\frac{\beta_P}{\beta_R}\right)\text{Ray} + \left(\frac{\beta_A}{\beta_R}\right)\text{Mie} \tag{23}$$

where β_R = volume scattering function for air molecules.
When this expression is rewritten as a product of two factors

$$\left(\frac{\beta_A}{\beta_R}\right)\text{Obs} = \left(\frac{\beta_A}{\beta_R}\right)\text{Mie}\left(1 + \frac{\beta_P}{\beta_A}\right) \tag{24}$$

we see that when $\beta_P > 0$, the measured turbidity is greater than that due to Mie particles alone by the factor in brackets. Moreover, the ratio (β_P/β_A) provides an additive term that indicates the relative contribution of small particles versus large particles. In principle then, if β_P is greater than β_A this term is indeed not negligible. To obtain a qualitative estimate of the magnitude of this factor consider the following:

From Eq. (15) an exponential distribution of Mie particles with $\nu = 4$ would give a scattering function proportional to λ^{-2}. A similar power-law distribution of Rayleigh particles has $\nu = 6$ and a λ^{-4} wavelength factor. (Note that this distribution is the same as the log-normal distribution in

---

20. Rossler, F. (1972) Aerosol layers in the atmosphere, *Space Research XII* **29**:423-431.
21. Pilipowsky, S. et. al. (1968) Investigation of the stratospheric aerosol by infrared and Lidar techniques, *J. Geophys. Res.* **73**:7553-7560.

Section 3.2 for small particles). If the index of refraction is approximately the same for both distributions [and at $\phi \simeq 50°$ the phase functions are nearly equal, see Eq. (3)] we have

$$\frac{\beta_P}{\beta_A} \simeq (2\pi)^2 \frac{6}{4} \frac{N_P}{N_A} \frac{r_P^6}{r_A^4} \frac{\lambda^{-4}}{\lambda^{-2}} = 59 \frac{N_P}{N_A} \left(\frac{r_P}{r_A}\right)^4 \frac{r_P^2}{\lambda^2} \tag{25}$$

when

N_P = number or Rayleigh particles with radius r_P

N_A = number of Mie particles with radius r_A.

Now if $r_P = 0.05$ μm and $r_A = 0.2$ μm and $\lambda = 0.475$ μm we obtain

$$\frac{\beta_P}{\beta_A} = \frac{N_P}{N_A} (2.56 \times 10^{-3}) . \tag{26}$$

For $\frac{\beta_P}{\beta_A} > 2$, it is only necessary that $\frac{\beta_P}{\beta_A} > 10^3$, with the implication that 10^3 Rayleigh particles are required to give twice the scattering intensity of 1 Mie particle. The next question is how does such a factor $(\beta_P/\beta_A) > 2$ affect the turbidity-wavelength dependence? Since the balloon-borne nephelometer provided simultaneous measurements at different wavelengths, Eq. (24) can be employed to determine the turbidity quotient for two wavelengths. In particular it is desirable to establish a condition under which the observed turbidity at 0.475 μm is greater than that observed at 0.660 μm. A ratio of such turbidities from Eq. (24) is

$$\frac{(\beta_A/\beta_R)\ \text{obs} \cdot \lambda_1}{(\beta_A/\beta_R)\ \text{obs} \cdot \lambda_2} = \left[\frac{(\beta_A/\beta_R)\ \text{Mie}\ \lambda_1}{(\beta_A/\beta_R)\ \text{Mie}\ \lambda_2}\right] \left[\frac{1 + (\beta_P/\beta_A)\ \lambda_1}{1 + (\beta_P/\beta_A)\ \lambda_2}\right] . \tag{27}$$

Now we have seen previously that β_A = (constant) λ^{-2} when $\nu = 4$, where the constant factor is independent of λ even though it is a function of the particle size distribution. Moreover, at a designated altitude and molecular number density, β_R = (constant) λ^{-4}.

Thus $(\beta_A/\beta_R)\ \text{Mie} = (C_A/C_R)\ \lambda^2$ (28)

provides the λ-dependence for the factor in the turbidity due to Mie particles. Since the same particles are scattering light at both wavelengths we get

$$\frac{(\beta_A/\beta_R)\ \text{Mie}\ \lambda_1}{(\beta_A/\beta_R)\ \text{Mie}\ \lambda_2} = \left(\frac{\lambda_1}{\lambda_2}\right)^2 \tag{29}$$

and Eq. (27) becomes

$$\frac{(\beta_A/\beta_R)\ \text{Obs}\ \lambda_1}{(\beta_A/\beta_R)\ \text{Obs}\ \lambda_2} = \left(\frac{\lambda_1}{\lambda_2}\right)^2 \frac{1 + (\beta_P/\beta_A)\ \lambda_1}{1 + (\beta_P/\beta_A)\ \lambda_2} . \tag{30}$$

This quotient is greater than unity when

$$\frac{1 + (\beta_P/\beta_A)\ \lambda_1}{1 + (\beta_P/\beta_A)\ \lambda_2} > \left(\frac{\lambda_2}{\lambda_1}\right)^2 = 1.93, \text{ for } \lambda_1 = 0.475\ \mu\text{mm and } \lambda_2 = 0.660\ \mu\text{m} . \tag{31}$$

Further reduction of this expression leads to

$$(\beta_P/\beta_A)\,\lambda_1 > 0.93 + 1.93\,(\beta_P/\beta_A)\,\lambda_2\,. \tag{32}$$

This implies $(\beta_P/\beta_A)\,0.475\,\mu \geq 1.93$, when $(\beta_P/\beta_A)\,0.660\,\mu \leq \frac{1}{1.93} = 0.518$.

This condition is virtually the same as that suggested above when the number concentration of small particles is greater than that of large particles by a factor of 10^3. While in principle this example simply illustrates that the factor $[1 + \beta_P/\beta_A]$ in Eq. (24) due to Rayleigh particles has a wavelength dependence of approximately λ^{-2}, the number of small particles relative to large particles is the dominant physical quantity affecting (β_P/β_A). Consequently the instrumental capability to detect small particles is paramount. This situation can be surmised from Eq. (30) when $(\beta_P/\beta_A)\,0.660\,\mu << 1$, which is perhaps realistic for the 1970 nephelometer data as well as lidar systems operating at red wavelengths. In that case the right hand side of Eq. (30) is about 2 and is indeed consistent with the turbidity-wavelength profile in the troposphere in Figure 3.

Even though the size distribution of Mie particles was chosen for demonstration (and is not unique) the results indicate that high concentrations of small particles together with large particles cause a predictable effect on the turbidity-wavelength relationship. Therefore, the foregoing analysis appears to be a plausible explanation for the "unusual" dispersion observed. Furthermore, such an explanation is consistent with the high degree of polarization of the scattered light, also detected in the same altitude range.

3.4 Inferences from Angular Scattering Behavior

The observations from the flight in 1976 were examined in an effort to correlate the turbidity with altitudinal variations in angular scattering. The 1970 vertical profiles of forward-to-backward scattering were published previously[5] and showed similarities to the 1976 data, despite the observed turbidity dispersion. The method of analysis presented here is therefore applicable to the earlier data, but is complicated by the problem of separating the contribution to the turbidity from Rayleigh particles, because in principle only Mie particles cause changes in angular scattering symmetry. It is shown, however, in the next section that the similarities between these sets of data provide additional evidence for the reliability of the 1970 turbidity profiles, but the 1976 data offer a less complicated basis for considering Mie particle effects. Eq. (6) contains the Rayleigh phase function P_R, the aerosol phase function, P_A and turbidity τ. The 1976 profile of τ did not indicate "unusual" behavior in the troposphere like that experienced in 1970. That is, the wavelength dispersion is toward the red wavelength as predicted by Eq. (30) when $(\beta_P/\beta_A) << 1$ for all wavelengths. P_R in Eq. (6) therefore refers to molecular scattering and is usually expressed as

$$P_R(\phi) = \frac{3}{16\pi}\,(1 + \cos^2\phi)\,[sr^{-1}], \text{ and } \int_{4\pi}^{P_R} (\phi)d\Omega = 1 \tag{34}$$

where $d\Omega \equiv$ the element of solid angle. To facilitate comparison with published aerosol phase functions the normalized form used by Elterman[22] is more convenient, because it approaches unity at $\phi = 50°$. That is, $P_R = 3/4\,(1 + \cos^2\phi)$ and $P_R(30°) = P_R(150°) = 1.3$. Eq. (6) then becomes,

$$R = \frac{1.3 + \tau\, P_A(30°)}{1.3 + \tau\, P_A(150°)} \tag{35}$$

where $\tau = \frac{\sigma_A}{\sigma_R}$ is the turbidity determined from 50° intensity observations. Rearranging this expression gives

$$P_A(30°) = 1.3\,\frac{R-1}{\tau} + R\,P_A(150°)\,. \tag{36}$$

For a given size distribution of aerosol particles, the phase function changes very little with wavelength in the visible spectral range and to a first approximation $P_A(\lambda_1) = P_A(\lambda_2)$. For example the scattering function for the normal power-law particle size distribution was shown previously (see Eq. (15)) to contain a factor with the explicit wavelength dependence and the phase function, which is dimensionless. The phase function for the two wavelengths, λ_1 and λ_2, at a fixed angle, can differ by at most a small constant factor. While this factor may be significant in theory, it is virtually undetectable experimentally in view of the variability in the observed quantities R and τ as a function of altitude and wavelength. With this assumption that $P_A(\lambda_1) = P_A(\lambda_2)$, simultaneous measurements of R and τ at λ_1 and λ_2 provide two equations for $P_A(150°)$ in the quantity $P_A(150°)$ which can be solved to give

$$P_A(150°) = \frac{1.3}{(R_1 - R_2)}\left[\left(\frac{R_2 - 1}{\tau_2}\right) - \left(\frac{R_1 - 1}{\tau_1}\right)\right] \tag{37}$$

where R_1 = value of R at λ_1, R_2 = value of R at λ_2 and similar designations for the measured values of τ. This result, when used in Eq. (36) with either set of values for R and τ, indicates that $P_A(30°)$ and $P_A(150°)$ are determinable from the observed parameters. Interestingly, Eq. (37) places bounds on the experimental data because, for $P_A(150°) > 0$,

$$R_1 < \frac{\tau 1}{\tau 2}(R_2 - 1) + 1, \text{when } R_1 > R_2 \text{ and } \tau_1 > \tau_2\,. \tag{38}$$

This method was used to compute $P_A(30°)$ and $P_A(150°)$ at several altitudes from the vertical profiles of τ and R, to arrive at experimentally inferred angular scattering characteristics of aerosol particles encountered during the 1976 flight. The values are listed in Table 1. Because only two symmetric scattering angles were used, it is ambiguous and speculative to interpret the results in terms of well defined particle size distributions. Nevertheless, it is possible to make comparisons with theoretical models used by others.

---

22. Elterman, L. (1966) Aerosol measurements in the troposphere and stratosphere, *Appl. Opt.* **5**:1769-1775.

Table 1. Scattering Properties and Particle Number Concentrations (June 1976)

Altitude (km)	R_1	τ_1	R_2	τ_2	$P_A(30°)$	$P_A(150°)$	$P_A(30°)/P_A(150°)$	τ_1/τ_2	ν	$\frac{N(>0.15mm)}{cm^3}$	Mixing Ratio (particles/mg)
8	2.2	0.69	1.5	0.24	3.60	0.634	5.73	2.73	2.8	1.23	2.35
9	1.8	0.30	1.3	0.10	5.03	0.867	5.80	3.0	2.6	0.36	0.77
10	2.0	0.40	1.4	0.14	4.88	0.833	5.85	2.86	2.8	0.52	1.24
11	3.3	3.6	2.2	1.2	2.22	0.422	5.26	3.0	2.6	3.4	9.09
12	2.2	0.9	1.3	0.20	2.26	0.24	9.42	4.0	2.0	0.61	1.84
13	2.0	1.0	1.3	0.25	2.04	0.37	5.51	4.0	2.0	0.51	1.97
14	2.1	1.11	1.5	0.37	2.92	0.78	3.74	3.0	2.6	0.66	2.55
15	2.5	1.47	1.5	0.43	1.79	0.185	9.67	3.41	2.3	0.56	2.46
16	3.2	2.1	1.7	0.50	2.34	0.305	7.67	4.02	2.0	0.76	3.94
17	4.0	3.8	2.1	1.0	1.87	0.212	8.84	3.8	2.0	1.18	7.30
18	4.18	3.5	2.2	1.01	1.94	0.182	10.67	3.46	2.2	0.83	6.11
19	4.7	3.7	2.3	1.10	1.76	0.098	17.96	3.36	2.3	0.75	6.57
20	4.4	3.2	2.6	1.20	2.24	0.196	11.43	2.67	3.0	0.97	10.08
21	3.2	3.8	2.0	1.30	1.41	0.206	6.84	2.92	2.7	0.98	12.07
22	3.05	3.17	2.2	1.50	1.55	0.234	6.62	2.11	3.7	0.88	12.81
23	4.4	5.0	3.0	1.60	3.21	0.529	6.07	3.13	2.5	0.70	12.03
24	2.5	2.8	2.1	1.80	1.31	0.245	5.35	1.56	4.6	0.56	11.34
25	3.5	5.3	2.5	2.0	1.88	0.362	5.19	2.65	3.0	0.70	16.70
26	2.6	4.9	1.8	2.0	0.729	0.119	6.17	2.5	3.2	0.60	16.80

Since the explicit relationship between scattering intensity and wavelength for a power-law particle size distribution provides a means to estimate particle number density, Eq. (15) was again employed to examine the turbidity-wavelength data. By rearrangement and change of notation, Eq. (15) takes the form

$$N \simeq \frac{\beta_A}{\nu}\left(\frac{\lambda}{2\pi r}\right)^{\nu}\left(\frac{2\pi}{\lambda}\right)^2 \frac{1}{P_A(50°)} \ [cm^{-3}] \ . \tag{39}$$

The factor $\eta(\phi,\lambda)$ in Bullrich's notation in Eq. (15) corresponds to the aerosol phase function $P_A(50°)$. Now, $\beta_A = \tau\beta_R$, where τ is the turbidity determined from the 50° scattering intensity and β_R is the Rayleigh scattering function. (The factor 2 was dropped because the measured intensity is the average of the polarized components). Assuming that the aerosol and Rayleigh phase functions are approximately equal near 50° scattering angle for clear air, $P_A(50°)$ is simply a relative factor that normalizes the aerosol phase function to the Rayleigh value of 1.06 at 50°, and renders the number of particles independent of scattering angle.

The exponent ν, at a particular altitude, is determined from the wavelength dependence of β_A (via τ) using the Angstrom formula, mentioned previously. That is,

$$\beta_A = \text{constant } \lambda^{-\alpha} \text{ and } \beta_R \sim \lambda^{-4}$$

so that $\tau \sim \lambda^{(-\alpha+4)} = \lambda^{(6-\nu)}$ since $\alpha = \nu - 2$ and $2 < \nu < 6$. It follows then that the turbidity has a positive wavelength exponent, α'.

$$\tau \sim \lambda^{\alpha'} \text{ where } \alpha' = 6 - \nu \text{ and therefore } 0 \le \alpha' \le 4$$

The exponent ν in the particle size distribution can thus be estimated from the quotient of turbidities measured at λ_1 and λ_2: That is,

$$\frac{\tau 1}{\tau 2} = \left(\frac{\lambda_1}{\lambda_2}\right)^{\alpha} \text{ and } \nu = 6 - \left(\frac{\log(\tau 1/\tau 2)}{\log(\lambda 1/\lambda 2)}\right).$$

The angular scattering phase functions for commonly used exponential size distribution have been computed from Mie Theory[13]. Consequently, aerosol particle concentrations that give rise to measured values of β_A can be estimated by using Eq. (39).

Such a procedure is deemed reasonable because as Harris and McCormick[23] have demonstrated, for a specific range of particle radii, a power-law size distribution can be approximated by a log-normal distribution; (shown in Section 3.2). Then too, an exponential wavelength dependence reflected in the scattering intensity implies that a power-law size distribution can be assumed without loss of generality because the angular scattering factor, although a function of size parameter, is not an explicit function of wavelength. The latter assertion was used as an assumption previously, but Eq. (39) clearly demonstrates from a dimensional perspective that $P_A(\phi)$ is independent of λ. As a first approximation then, the aerosol particle concentration at representative altitudes can be inferred from the turbidity data. In this connection, the 50° normalization factors, $P_A(50°)$, were determined by extrapolation from aerosol phase functions tabulated by Bullrich for a power-law size distribution of radii in the range (0.04 μm < r < 10 μm). These were deemed suitable for order-of-magnitude estimates and are listed in Table 2, along with the foreward-to-backscatter ratio. However, the latter ratio is dependent upon the upper and lower limits of radii used in the model and therefore varies with this range interval, which is an unknown in the nephelometer data. Specifically, a given exponent ν does not uniquely define the phase function and a strict comparison between the experimentally observed ratios and those in Table 2 cannot be made.

Table 2. Theoretical Scattering Parameters vs Power Law Exponent

ν	$P_A(50°)$	$P_A(30°)/P_A(150°)$
2.5	2.3	13.95
3.0	1.2	13.88
3.5	0.78	12.52
4.0	0.52	10.04

Figure 7a is an altitude profile of number of particles per cm^3 greater than 0.15 μm in radius, resulting from the conversion of turbidity at 0.660 μm to number density by using Eq. (39). Table 1 lists these data. To illustrate a typical calculation, the turbidity ratio (for 0.660 μm and 0.475 μm) at 9 km is about 3, which in turn implies $\beta_A \sim \lambda^{-0.6}$ or ν = 2.6.

Additionally, the observed value of τ (at 0.660 μm) is 0.3 and $\beta_R = 1.84 \times 10^{-9}$ cm^{-1} sr^{-1}. When these values are used in Eq. (39) we obtain at 9 km,

---

23. Harris, F.S. and McCormick, M.P. (1972) Mie scattering by three polydispersions, *J. Coll. and Inter. Sci.* **29**:536-545.

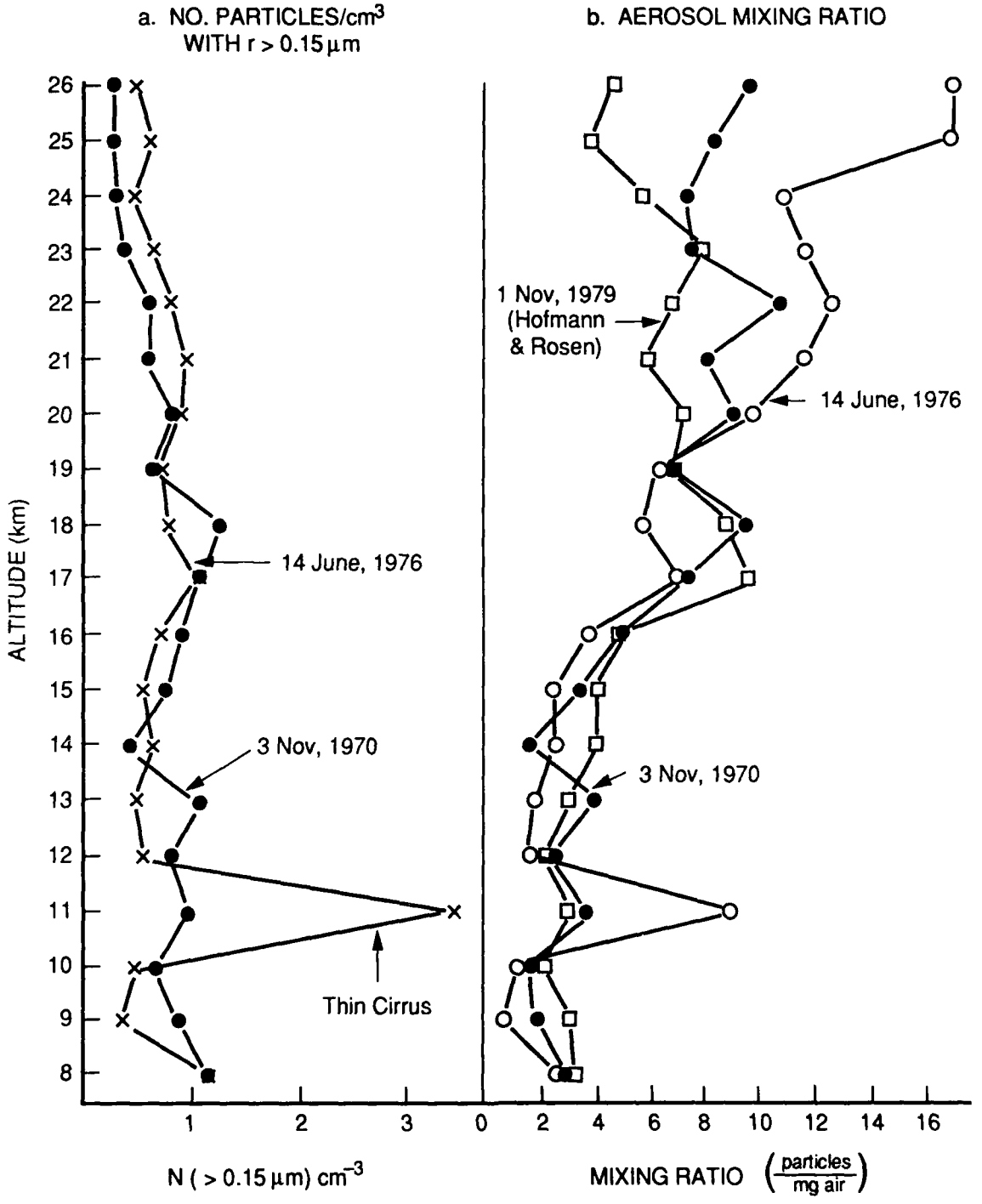

Figure 7. (a) Number of Particles vs Altitude, (b) Particle Mixing

$$N \simeq 0.3 \frac{\text{particles}}{\text{cm}^{-3}} \; (> 0.15\ \mu\text{m radius}) .$$

Extensive measurements by Hofmann and Rosen[24] using balloon-borne particle counters provide perhaps the best set of data available for comparison. In particular, their findings address the question of the aerosol background during non-volcanic periods and the altitudinal variability in the concentration of particles greater than 0.15 μm in radius. Their data are presented in terms of the aerosol mixing ratio, which is the quotient of the number of particles to air mass-density, and is defined by

$$\text{Aerosol Mixing Ratio} \equiv \frac{\text{particles/cm}^3}{\text{milligrams of air/cm}^3} = \frac{\text{particles}}{\text{milligrams}} .$$

The air mass-density is given in the tables of the Standard Atmosphere 1976. The relevance of the profile of the aerosol mixing ratio lies in its comparison with the the optical turbidity which is proportional to the number of aerosol particles per air molecule. When the number concentrations that were inferred from the turbidity measurements were converted to aerosol mixing ratio, Figure (7b) was obtained. This profile compares favorably with the data of Hofmann and Rosen obtained in 1979 over Laramie, Wyoming, and also shown in Figure (7b). Specifically, they found peak mixing ratios between 10 and 20 particles/milligrams in the stratospheric Junge layer between 18 and 23 km altitude along with an increase in relative concentration of small particles above 25 km. However, wide variability in size and mixing ratio was observed in the troposphere with significant seasonal dependence. For example, in the spring of 1978 when the peak mixing ratio for the stratosphere was about 8 particles/milligram, the ratio 10 km varied by at least an order of magnitude, from 2 to 20 particles/milligram. This contrast with the autumn values of about 0.5 to 2 in the 9 to 10 km level and the stratospheric values remained virtually unchanged. And again, the 1978-79 period was one in which volcanic dust influences were noticeably absent from their data. The high degree of variability in the tropospheric aerosols appears to be consistent with the nephelometer data presented in this report.

As noted above, the particle concentrations displayed in Figure (7a) refer to particles greater than 0.15 μm for an assumed power-law exponent in the size distribution. The dissymmetry parameter, on the other hand, is a measure of the effect of all particles encountered and without additional information related to particle size, could not be expected to provide strict comparison with the theoretical model used in determining particle number densities. From a qualitative viewpoint, however, the compatibility of these independent sets of data in presenting signatures for the presence of aerosols is evident. Within the margins of experimental error, the angular scattering as depicted in the R-parameter gives a reasonable picture of the change in the aerosol phase function with altitude in that the ratios are less limited to values characteristic of particles with radii less than about 0.2 μm. This can be ascertained from Van de Hulst[10] wherein the forward-to-backward scattering by a sphere is tabulated as a function of size parameter and the magnitude of the forward enhancement as a function of particle size can be estimated. His Table 5 Section 7.22, indicates that

---

24. Hofmann, D.F. and Rosen, J.M. (1981) On the background stratospheric aerosol layer, *J. Atmos. Sci.* **38**:168-181.

for size parameters less than 2, the total scattering in the forward hemisphere exceeds that in the backward hemisphere by a factor less than 10.70, but rapidly increases to a factor of 62.0 when the size parameter reaches 3. Similarly, a size distribution such as Deirmendjian's continental haze model[25] results in a factor 16.5 as the ratio between the value of phase functions at 30° and 150°. Other models of atmospheric aerosols such as Elterman[22], for visibility conditions of at least 30 km, also indicate this factor lies in a range from 10-20, depending upon the relative weighting of particles with radii greater than 0.2 μm. The inferred phase functions in Table 1 are reasonably close to these models. Notably, the relative change in $P_A(150°)$ is more pronounced at the stratospheric altitude of 18 km than in the troposphere, which is consistent with an increase in particle size in the Junge layer. The LOWTRAN aerosol phase functions[26] illustrate this behavior of the backscatter, for a wide variety of atmospheric aerosol models. Therefore, the absolute precision in values for the dissymmetry does not preclude an informative correlation of this parameter with substantive angular scattering properties of aerosols, and reasonable inferences relating to particle size can be made from such data.
The dissymmetry parameters for the 1970 data are displayed in Figure 8 from ground-level to 15 km altitude (due to failure of the backscatter photometer at 15 km). Those results are consistent with the 1976 data in which a comparable wavelength relationship existed, namely dispersion toward the longer wavelengths. However, in Figure 8, the R-values for the 0.475 μm wavelength remained less than about 1.45 in the troposphere (from 5-15 km) indicating virtually constant symmetry; a property of Rayleigh scattering. Such symmetry was absent at 0.660 μm, thereby strengthening the suggestion made in Section 3.3 that this wavelength was insensitive to the small particle component in the aerosol distribution. On the contrary, the 1976 data in Figure 6 do not show such constant R-values for the blue wavelength. Apparently, both the subtle differences and distinct similarities between the sets of data reveal physically significant aspects of angular scattering from atmospheric particles encountered. Specifically, the disparity in the magnitude of variability in the vertical profiles indicates the contrasting size ranges of tropospheric particles, despite the compatibility in wavelength displacement.

In the next section, a connection between the dissymmetry and polarization is made, which correlates the primary scattering characteristics of small particles. This correlation provides a more quantitative resolution of the problem of the "unusual" turbidity/wavelength behavior evident in the 1970 data. In particular, the polarization of the scattered light can be used to separate the small particle component from the total scattering intensity. This, in turn, facilitates a comparison of the size distribution of large particles observed for the two contrasting sets of data.

3.5 Inferences from the Polarizing Properties of Small Particles

Perhaps the most interesting data from the 1970 balloon flight was the polarization of the scattered light at the 90° scattering angle. In addition to angular symmetry, light scattered by small particles is polarized to a greater degree than that by large particles. Therefore, the observed

---

25. Deirmendjian, D. (1969) *Electromagnetic Scattering in Polydispersions*, Elsevier, New York.
26. Kneizys, F.X. et. al. (1983) *Atmospheric Transmittance/Radiance: Computer Code LOWTRAN 6*, AFGL-TR-83-0187, ADA137786.

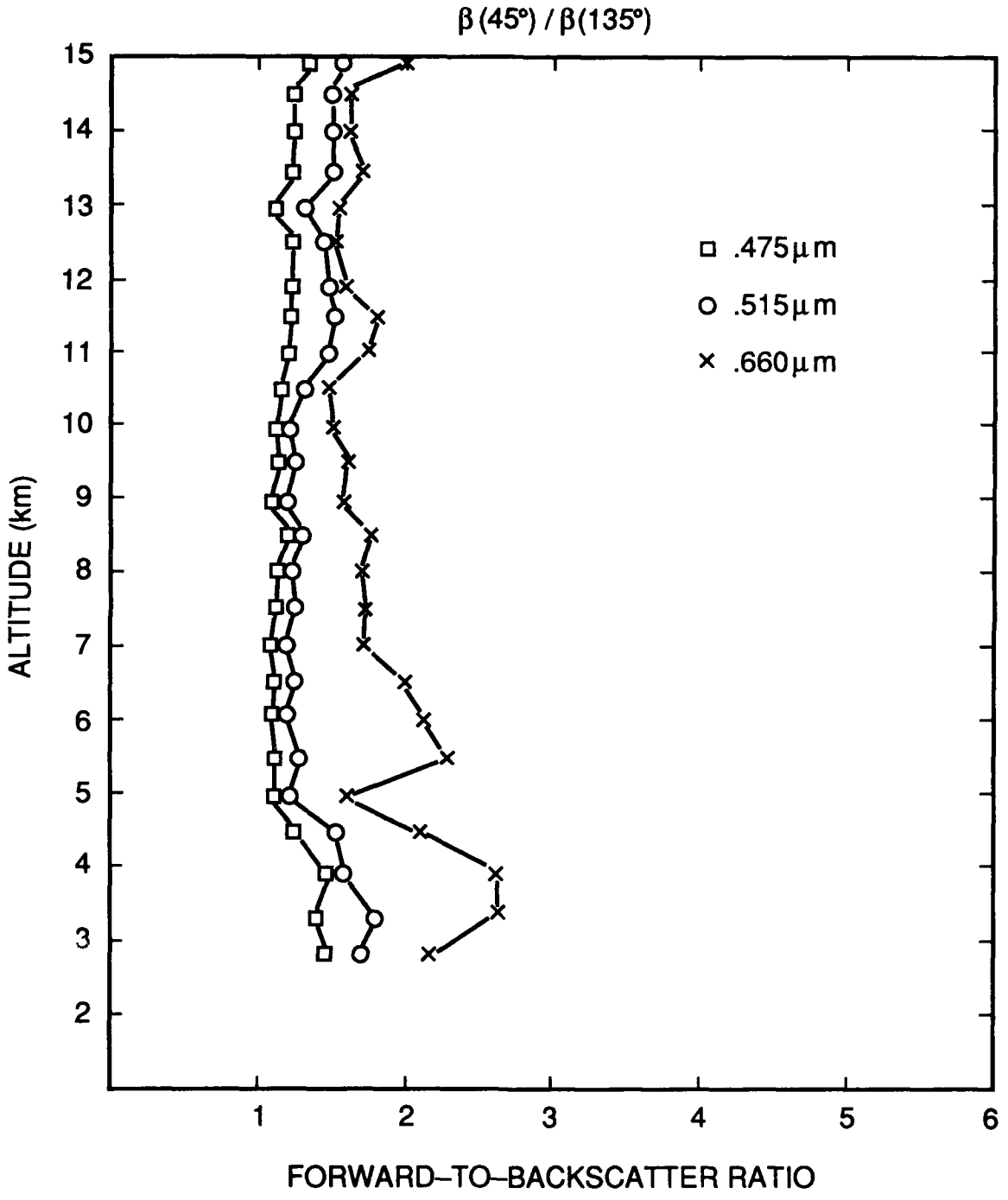

Figure 8. The Ratio of Forward-to-Backward Scattering (Dissymmetry) vs Altitude (November 1970)

polarization ratio at 0.475 μm, Figure 5, can be used to examine this behavior in the troposphere. Call[27] suggested a procedure for investigating the relationship between polarization and aerosol particle size, using a LIDAR system. His technique was adapted to the nephelometer observations in the following manner: For a particular photometer, the photomultiplier (PM) detector response is linearly related to the volume scattering function and can be expressed as,

$$W(\phi_s) = K\ \beta_\lambda\ (\phi_s) \tag{41}$$

where K is the calibration factor for a photometer at scattering angle ϕ_s with spectral filter of wavelength, λ. From Eq. (2) this can be written

$$W(\phi_s) = K\left[\sigma_{R\lambda}\ P_R(\phi_s) + \sigma_{A\lambda}P_A(\phi_s) + \sigma_{P\lambda}\ P_R(\phi_s)\right] \tag{42}$$

where $\sigma_{P\lambda}$ is the scattering coefficient due to small particles, which are also assumed to have a Rayleigh scattering phase function $P_R(\phi_s)$. The other terms were defined previously in connection with Eq. (2). The PM tube is insensitive to the polarization of the scattered light, but the vertical and horizontal polarized intensities can be detected sequentially with properly oriented polarizers. The balloon-borne photometers used this arrangement. The detector responses then take the form

$$I_V(\phi_s) = CW_V(\phi_s) = K_1[\sigma_{R\lambda}P_{RV}(\phi_s) + \sigma_{A\lambda}P_{AV}(\phi_s) + \sigma_{P\lambda}P_{RV}(\phi_s)] \tag{43}$$

and

$$I_H(\phi_s) = CW_H(\phi_s) = K_1[\sigma_{R\lambda}P_{RH}(\phi_s) + \sigma_{A\lambda}P_{AH}(\phi_s) + \sigma_{P\lambda}\ P_{RH}(\phi_s)] \tag{44}$$

where K_1 is a constant which includes the linear relationship between the PM tube response and the intensity. The subscripts V and H on the respective phase functions simply refer to the vertical and horizontal components. Note that the scattering coefficients σ are independent of scattering angle. The ratio of Eq. (43) to Eq. (44) gives a quantity with the calibration factor eliminated, and is simply the polarization ratio,

$$\frac{I_V(\phi_s)}{I_H(\phi_s)} = \frac{\sigma_{R\lambda}\ P_{RV}(\phi_s) + \sigma_{A\lambda}P_{AV}(\phi_s) + \sigma_{P\lambda}\ P_{RV}(\phi_s)}{\sigma_{R\lambda}\ P_{RH}(\phi_s) + \sigma_{A\lambda}P_{AH}(\phi_s) + \sigma_{P\lambda}\ P_{RH}(\phi_s)}\ . \tag{45}$$

At $\phi_s = 90°$ this expression is simplified, because P_{RH} (90°) is proportional to $\cos^2\phi_s$, which equals zero at $\phi_s = 90°$. Therefore for the photometer at $\phi_s = 90°$ we obtain

$$\frac{I_V}{I_H} = \frac{\sigma_{RH}P_{RV}(90°)}{\sigma_{A\lambda}P_{AH}(90°)} + \frac{P_{AV}(90°)}{P_{AH}(90°)} + \frac{\sigma_{P\lambda}\ P_{RV}(90°)}{\sigma_{A\lambda}P_{AH}(90°)}\ . \tag{46}$$

Using the relationship

$$\frac{\sigma_{p\lambda}}{\sigma_{A\lambda}} = \frac{\sigma_{p\lambda}}{\sigma_{R\lambda}} \cdot \frac{\sigma_{R\lambda}}{\sigma_{A\lambda}} \tag{47}$$

---

27. Call, R. (1967) *Measurement of Atmospheric Aerosols by Polarized-Laser Light Scattering*, Univ. Microfilms, Inc., Ann Arbor, MI.

we get

$$\frac{I_V}{I_H} = \frac{\sigma_{R\lambda}}{\sigma_{A\lambda}}\left(1 + \frac{\sigma_{P\lambda}}{\sigma_{R\lambda}}\right)\frac{P_{RV}(90°)}{P_{AH}(90°)} + \frac{P_{AV}(90°)}{P_{AH}(90°)} . \tag{48}$$

Finally,

$$(1 + \sigma_{P\lambda}/\sigma_{R\lambda}) = \frac{I_V/I_H - P_{AV}(90°)/P_{AH}(90°)}{P_{RV}(90°)/P_{AH}(90°)} \frac{\sigma_{A\lambda}}{\sigma_{R\lambda}} . \tag{49}$$

This result shows that the small particle turbidity factor, $(1 + \sigma_P/\sigma_R)$ can be determined from the polarization ratio and is directly related to the turbidity, σ_A/σ_R. It is important to note that at $\lambda = 0.475$ μm, this value of σ_A/σ_R arises from both small particles and large particles and can be equated to the observed value at the 45° scattering angle, since σ is independent of scattering angles. For example if $\sigma_P = 0$; that is, there are no small particles, the turbidity due to large particles alone is from Eq. (49)

$$(\sigma_A/\sigma_R)_{\sigma P=0} = \frac{P_{RV}/P_{AH}}{(I_V/I_H)_0 - P_{AV}/P_{AH}} . \tag{50}$$

The observed turbidity is therefore

$$(\sigma_A/\sigma_R)_{obs} = (\sigma_A/\sigma_R)_{\sigma P=0}\,(1 + \sigma_P/\sigma_R)\,\frac{(I_V/I_H)_0 - (P_{AV}/P_{AH})}{(I_V/I_H) - (P_{AV}/P_{AH})} . \tag{51}$$

It is thus evident that the observed turbidity is greater than that due to large particles alone when

$$(1 + \sigma_P/\sigma_R) > \frac{I_V/I_H - P_{AV}/P_{AH}}{(I_V/I_H)_0 - P_{AV}/P_{AH}} \tag{52}$$

or

$$\sigma_P/\sigma_R > \frac{I_V/I_H - (I_V/I_H)_0}{(I_V/I_H)_0 - P_{AV}/P_{AH}} . \tag{53}$$

A further implication from Eq. (50) and this inequality is that

$$(\sigma_A/\sigma_R)_{\sigma P=0} < \frac{(\sigma_P/\sigma_R)\,P_{RV}/P_{AH}}{I_V/I_H - (I_V/I_H)_0} . \tag{54}$$

It is evident therefore, that the aerosol turbidity factor $(\sigma_{A\lambda}/\sigma_{R\lambda})$ in Eq. (49) is a function of the relative concentrations of small particles which cause the enhanced polarization ratio.

Inspection of Figure 5 indicates that near ground level and in the stratosphere (altitude > 16 km), both regions where large particles were dominant, I_V/I_H is less than 6. On the other hand, this ratio reaches values between 8 and 10 in the troposphere, where the small particle contribution to both the polarization and turbidity must be considered. Now, Eq. (49) provides a means to determine the factor $(1 + \sigma_P/\sigma_R)$, at 0.475 μm, from the observables I_V/I_H and (σ_A/σ_R) if suitable aerosol phase functions can be found. Particularly applicable in this connection were phase functions used by Call[27] in his LIDAR work, because he derived and plotted the two polarized components as a function of scattering angle. He assumed an exponential size distribution and refractive index of 1.5 for the aerosol particles. The pertinent parameters, giving the best fit to the measured data are given in Table 3.

Table 3. Theoretical Polarization Parameter vs Power-Law Exponent

ν	Size Range	$P_{Rv}(90°)/P_{AH}(90°)$	$P_{Av}(90°)/P_{AH}(90°)$
3.5	$.1 < r < 1\ \mu m$	7.93	2.35
3.0	$.1 < r < 1\ \mu m$	7.53	1.84
2.5	$.1 < r < 1\ \mu m$	7.00	1.35

To identify the proper phase function at a particular altitude, the dissymmetry parameter provides a source for testing the data consistency because it also contains the small particle parameter, $(1 + \sigma_P/\sigma_R)$. This condition arises in a manner similar to Eq. (6) when the small particles are included. That is, in view of the assumption that the small particles are Rayleigh scatterers and thus have the same phase function as air molecules, the ratio of forward-to-backward scattering intensities is now

$$R = \frac{(1 + \sigma_P/\sigma_R)\ P_R(45°) + (\sigma_A/\sigma_R)\ P_A(45°)}{(1 + \sigma_P/\sigma_R)\ P_R(135°) + (\sigma_A/\sigma_R)\ P_A(135°)} \tag{55}$$

where the symmetric scattering angles for the 1970 data were 45° and 135°. In this case the $(1 + \cos^2 \phi_S)$ Rayleigh factor gives $P_R(45°) = P_R(135°) = 1.12$ and Eq. (55) becomes

$$R = \frac{1.12\ (1 + \sigma_P/\sigma_R) + \tau P_A(45°)}{1.12\ (1 + \sigma_P/\sigma_R) + \tau P_A(135°)} \tag{56}$$

and $\tau = (\sigma_A/\sigma_R)$ is the turbidity due to large (Mie) particles alone as observed with the photometer at 45°. Rearranging this expression gives

$$P_A(45°) = 1.12\ (1 + \sigma_P/\sigma_R) \left(\frac{R - 1}{\tau}\right) + R\, P_A(135°) \tag{57}$$

and with the assumption that the phase function is independent of wavelength, used previously in Section 3.4, we arrive at an expression analogous to Eq. (37)

$$P_A(135°) = \frac{1.12}{R_1 - R_2}\ [1 + \sigma_P/\sigma_R] \left[\left(\frac{R_2 - 1}{\tau_2}\right) - \left(\frac{R_1 - 1}{\tau_1}\right)\right]. \tag{58}$$

This relation assumes that τ_1 is due to only Mie particles. In the interpretation of the 1970 turbidity data, (Figure 3), it was asserted that the observed values of τ_2 at 0.475 μm were masked by the small particles in the troposphere. To apply Eq. (58) it is necessary to infer the probable values of τ_2 from those at $\lambda = 0.660$ μm, by assuming a turbidity-wavelength dependence consistent with the polarization data. That is, the choice of aerosol phase function that best matches the polarization and turbidity parameters in Eq. (49) establishes the exponent ν in the size distribution as well as the λ-dependence in the turbidity from the relation

$$\tau \sim \lambda^{6-\nu} \text{ and thus } \frac{1}{\tau_2} = \frac{1}{\tau_1}\left(\frac{\lambda_1}{\lambda_2}\right)^{6-\nu}. \tag{59}$$

Equation (58) can finally be expressed in terms of the ν and τ_1, the observed turbidity at $\lambda = 0.660$ μm.

$$P_A(135°) = \frac{1.12}{R_1 - R_2} \frac{[1 + \sigma_P/\sigma_R]}{\tau_1} \left[(R_2 - 1) \left(\frac{\lambda_1}{\lambda_2} \right)^{6-\nu} - (R_1 - 1) \right]. \quad (60)$$

Again, this expression is quite sensitive to the exponent ν, which cannot be chosen arbitrarily if the data are to be consistent and because

$$\left(\frac{\lambda_1}{\lambda_2} \right)^{6-\nu} > \frac{R_1 - 1}{R_2 - 1} \quad (61)$$

if the $P_A(135°)$ has positive values.

This procedure was employed to examine the variability in aerosol phase functions up to only 15 km for the 1970 data because of the failure of the 135° photometer previously mentioned. Moreover, initial guidance for making judicious selection of values of ν comes from the fact that the values of τ and R at 0.660 μm were comparable for both flights in 1970 and 1976. This suggested that the size distributions of large particles were not appreciably different in the troposphere. The analytical procedures thus involved three steps. First, an estimate of the ν-value satisfying condition (61) was made. Second, this value defined the phase function used in Eq. (49) at a particular altitude, to determine $(1 + \sigma_P/\sigma_R)$ from the observables I_V/I_H and (σ_A/σ_R). Third, the value so determined was used to find $P_A(135°)$ from Eq. (60) and subsequently $P_A(45°)$ from Eq. (57). Finally, in the same manner as in Section 3.4, it was possible to estimate the number of particles greater than 0.15 μm for a given ν-value from the observed turbidity values at 0.660 μm. Table 4 lists the values of the above parameters for the 1970 flight. Included in the table is the small particles turbidity, $\tau_P = \sigma_P/\sigma_R$ and two other quantities; the number of small particles (radius > 0.04 μm) per cubic centimeter, and the small particle mixing ratio. The number concentration of small particles can be estimated from Eq. (39) by substituting the parameter values; $\beta_P = \tau_P\ \beta_R$, λ = 0.475 μm, r = 0.04 μm, ν = 6 and $P_R(45°) = 1.12$. As for

Table 4. Scattering Properties and Particle Number Concentrations (November 1970)

Altitude (km)	R_1	τ_1	R_2	τ_2 (Cal)	σ_P/σ_R (t_P)	$P_A(45°)$	$P_A(135°)$	$\frac{P_A(45°)}{P_A(135°)}$	τ_1/τ_2	ν	$\frac{N>0.15\ mm}{cm^2}$	Mixing Ratio $\frac{(N>0.15\ mm)}{mg}$	$\frac{N>0.04\ mm}{cm^2}$	Mixing Ratio $\frac{(N>0.04\ mm)}{mg}$
3	2.20	1.9	1.50	0.71	1.10	2.04	0.25	8.16	2.68	3.0	3.50	3.98	1800	2050
4	2.15	1.8	1.45	0.63	1.22	2.19	0.28	7.82	2.87	2.8	3.20	4.03	1837	2312
5	1.70	1.0	1.25	0.40	1.40	2.46	0.44	5.59	3.17	2.5	2.18	3.04	1792	2503
6	2.15	1.2	1.35	0.48	1.24	3.12	0.33	9.45	3.17	2.5	1.40	2.31	1426	2214
7	1.70	1.1	1.25	0.44	1.40	2.46	0.44	5.59	3.17	2.5	1.59	2.74	1477	2542
8	1.68	0.9	1.25	0.35	0.80	2.11	0.40	5.27	3.06	2.6	1.23	2.35	740	1378
9	1.60	0.7	1.20	0.28	0.85	2.18	0.25	8.72	3.17	2.5	0.87	1.86	715	1481
10	1.50	0.8	1.20	0.30	0.63	1.49	0.23	6.48	2.65	3.0	0.69	1.64	459	1093
11	1.76	1.2	1.30	0.39	0.80	2.30	0.58	3.96	3.06	2.6	1.04	2.78	513	1372
12	1.70	1.3	1.35	0.49	0.80	2.29	0.71	3.22	2.65	2.8	0.84	2.53	442	1331
13	1.50	1.2	1.20	0.38	0.74	1.91	0.73	2.61	3.17	2.5	1.17	3.98	344	1170
14	1.75	1.2	1.40	0.53	0.46	2.14	0.63	3.40	2.28	3.5	0.41	1.58	187	122
15	1.95	1.3	1.40	0.49	0.19	1.46	0.20	6.80	2.65	3.0	0.78	3.43	60	263

large particles, the small particle mixing ratio is simply the quotient of the number concentration divided by the air mass density.

It is readily apparent from Table 4 that the number concentration of small particles exceeds the large particle concentration by a factor of at least 0.5×10^3, in the altitude range 5 -12 km. This result is consistent with the qualitative estimates deduced from Eq. (25) in Section 3.3, when allowance is made for the v-values, indicated for the large particles. That is, the latter values are less than 3, while Eq. (25) assumed $v = 4$.

In the 8 -15 km region, the large particle concentrations for the two flights are closely comparable. (No data were used below 8 km for the 1976 flight, because the balloon ascent rate was too rapid.)

This region is particularly significant, however, because it has been previously identified as one in which backscatter from ground based LIDAR systems reached minimum values, and was thus considered appropriate for data normalization purposes[28].

4. CONCLUSIONS

The nephelometer scattering observations provide self-consistent vertical profiles of aerosol scattering effects in the troposphere and stratosphere. The optical properties of the stratosphere over New Mexico showed little change from 1970 to 1976 even though the intervening period included a major volcanic dust event and the rare observation of a nacreous cloud at 25 km[6]. By contrast, however, the troposphere exhibited wide variability, including evidence of optical scattering effects attributable to the gamut of aerosol particles from condensation nuclei to Mie particles even in presumably clear air. In particular the data suggest that small particles that exhibit Rayleigh scattering cannot be neglected in a realistic picture of aerosol optical effects in the atmosphere. That such particles may exist in large concentrations in a very clear sky is amply demonstrated by the formation of jet contrails, and indeed they are critical to the growth of clouds, as nucleating agents. The discrepancy between the results obtained with LIDAR probing and those from other atmospheric optical techniques, as pointed out by Rozenberg[29], finds further confirmation in the data from the nephelometer flights. Specifically, the values of optical turbidity observed were at least a factor of 2 greater than those determined by lidar during non-volcanic periods. Additionally, the nephelometer data showed an increase in turbidity and aerosol mixing ratio above 23 km, despite a reduction in concentration of particles with radii greater than 0.15 μm. This result is apparently consistent with the finding of Hofmann and Rosen[24] relating to increased numbers of small particles at altitudes above the Junge layer; a result not evident from atmospheric sounding with lidar, but clearly manifested in the occurrence of high altitude clouds.

The nephelometer observations support the finding by others indicating the existence of an ever-present background of aerosol particles in the earth's atmosphere against which the recent dust incursions from eruptions such as Mt St Helens and El Chichon should be measured. Morever, this background of aerosols has been shown to be somewhat self-sustaining and perhaps natural in origin.

---

28. Russell, P.B. et. al. (1979) Methodology for error analysis and simulation of Lidar aersosol measurements, *Appl. Opt.* **18**:3783-3797.

29. Rozenberg, G.V. and Sandormirsky, A.B. (1971) The optical stratification of atmospheric aerosols, *Izu. Atmospheric and Oceanic Physics* **7**:737-749.

although uncertainties remain as to a clear source, because of anthropogenic as well as continuing volcanic influences.

References

1. Northam, G.B. et. al. (1974) Dustsonde and lidar measurements of stratospheric aerosols: a comparison, *Appl. Opt.* **13**:2416-2421.
2. Russell, P.B. et. al. (1975) Results of stratospheric lidar observations, *Fourth Conference on the Climatic Impact Assessment Program*, Cambridge, MA, 4-7 February.
3. McCormick, M.P. and Fuller, W.H. (1975) Lidar measurements of intense stratospheric dust layers, *Appl. Opt.* **14**:4-5.
4. Barteneva, O.D. (1960) Scattering functions of light in the atmospheric boundary layer, *Bull. Acad. Sci. USSR Geophys. Sci.*, 1237-1244.
5. Gibson, F.W. and Dearborn, F.K. (1971) *Atmospheric Optics Measurements with a Balloon-Borne Nephelometer*, AFCRL-TR-71-0455, AD736408.
6. Gibson, F.W. and Volz, F.E. (1972) High altitude measurements of the optical-scattering properties of the atmosphere, presented at Optical Society of America Meeting, New York, NY, April.
7. Gibson, F.W. (1976) In-situ photometric observations of angular scattering from atmospheric aerosols, *Appl. Opt.* **15**:2520-2533.
8. Meinel, A.B. and Meinel, M.P. (1975) A stratospheric dust event of November 1974, *Science* **188**:477-481.
9. Junge, C.E., Chagnon, C.W., and Manson, J.E. (1961) Stratospheric aerosols, *J. Meteorol.* **18**: 81-98.
10. Van de Hulst, H.C. (1957) *Light Scattering by Small Particles*, John Wiley & Sons, New York.
11. Sassen, K. (1981) Infrared (10.6 μm) scattering and extinction in laboratory water and ice clouds, *Appl. Opt.* **20**:185-193.
12. Kerker, M. (1969) *The Scattering of Light and Other Electromagnetic Radiation*, Academic Press, New York.
13. Bullrich, K. (1964) Scattered radiation in the atmosphere and the natural aerosol, *Advances in Geophysics* **10**:101-257.
14. Junge, C.E. (1961) Vertical profiles of condensation nuclei in the stratosphere, *J. Meteorol.* **18**:501-509.

15. Went, F.W. (1964) The nature of Aitkin condensation nuclei in the atmosphere, *Nature* **51**:1259-1267.

16. Whitby, K.T. (1975) *Modeling of Atmospheric Aerosol Particle Size Distribution*, Prog. Rep. 253, Particle Technology Laboratory, Univ. of Minnesota, Minneapolis.

17. Junge, C.F. and McLaren, E. (1971) Relationship of cloud nuclei spectra to aerosol size distribution and composition, *J. Atmos. Sci.* **28**:382-390.

18. Nilsson, B. (1979) Meteorological influence on aerosol extinction in the 0.2 μm - 40 μm wavelength range, *Appl. Opt.* **18**:3457-3473.

19. Shettle, E.P. and Fenn, R. W. (1979) *Models for the Aerosol of the Lower Atmosphere and the Effects of Humidity Variations on their Optical Properties*, AFGL-TR-79-0214, ADA085951.

20. Rossler, F. (1972) Aerosol layers in the atmosphere, *Space Research XII* **29**:423-431.

21. Pilipowsky, S. et. al. (1968) Investigation of the stratospheric aerosol by infrared and Lidar techniques, *J. Geophys. Res.* **73**:7553-7560.

22. Elterman, L. (1966) Aerosol measurements in the troposphere and stratosphere, *Appl. Opt.* **5**:1769-1775.

23. Harris, F.S. and McCormick, M.P. (1972) Mie scattering by three polydispersions, *J. Coll. and Inter. Sci.* **29**:536-545.

24. Hofmann, D.F. and Rosen, J.M. (1981) On the background stratospheric aerosol layer, *J. Atmos. Sci.* **38**:168-181.

25. Deirmendjian, D. (1969) *Electromagnetic Scattering in Polydispersions*, Elsevier, New York.

26. Kneizys, F.X. et. al. (1983) *Atmospheric Transmittance/Radiance: Computer Code LOWTRAN 6*, AFGL-TR-83-0187, ADA137786.

27. Call, R. (1967) *Measurement of Atmospheric Aerosols by Polarized-Laser Light Scattering*, Univ. Microfilms, Inc., Ann Arbor, MI.

28. Russell, P.B. et. al. (1979) Methodology for error analysis and simulation of Lidar aersosol measurements, *Appl. Opt.***18**:3783-3797.

29. Rozenberg, G.V. and Sandormirsky, A.B. (1971) The optical stratification of atmospheric aerosols, *Izu. Atmospheric and Oceanic Physics* **7**:737-749.